Gottfried Wilhelm Leibniz Universität Hannover

Institut für Radioökologie und Strahlenschutz (IRS)

Determination of strontium-90 in food concentrates from Japan

Master thesis

Written by

Anica Weller

Supervisor:

Prof. Dr. Georg Steinhauser

Prof. Dr. Clemens Walther

Hanover, 29th March 2017

Danksagung

Zunächst möchte ich mich ganz herzlich bei Prof. Dr. Georg Steinhauser bedanken, der mich in seinen Arbeitskreis aufgenommen hat und mir die Möglichkeit gegeben hat, an diesem interessanten Thema zu arbeiten. Durch sein Engagement für das Thema und die gute Betreuung gab er mir viele hilfreiche Anregungen und Hilfestellungen zur Bearbeitung der Masterarbeit.

Des Weiteren danke ich Prof. Dr. Clemens Walther für die Übernahme der Zweitprüferschaft.

Ass.-Prof. Dr. Katsumi Shozugawa von der Universität von Tokyo gilt mein Dank für die Bereitstellung der 37 Lebensmittelproben, die aus verschiedenen Präfekturen aus Japan gesammelt wurden.

Ich möchte Rebecca Querfeld für ihre Mühe in die Einarbeitung in die verwendeten Geräte und Labore und die tatkräftige Unterstützung herzlichst danken.

Des Weiteren bedanke ich mich bei Dennis, Lennart, Jessica und Fabian für das Korrekturlesen der Arbeit.

Darüber hinaus möchte ich mich ganz herzlich bei allen Mitarbeitern des Instituts für Radioökologie und Strahlenschutz der Universität Hannover bedanken. Zu jederzeit halfen mir das Engagement und die Anregungen aus vielfältigen Richtungen zu einem tieferen Verständnis für die Radioökologie. Außerdem sorgten viele gesellschaftliche Aktivitäten wie Pasta, Freitagswurst und Spieleabende für ein unvergleichbar tolles Arbeitsklima.

Ein besonderer Dank gilt meiner Familie, meinen Freunden und meinem Freund, die mich in meinem Studium und in allen Lebenslagen unterstützt und motiviert haben.

Abstract

In this thesis, the radioactive fission product ^{90}Sr is analysed in food samples from Japan. Due to the nuclear accident at the Fukushima Daiichi nuclear power plant (NPP) on March 11, 2011, large amounts of radioactive substances were released into the environment. Especially the uptake and incorporation of radionuclides with food and drinking water is a high risk for the human health. Therefore, constant surveillance and analysis of possible contaminated foods are of high importance. As for the radionuclides ^{134}Cs, ^{137}Cs and ^{131}I, which are γ-emitters, good and straightforward monitoring using gamma spectroscopy is possible. In contrast, the measurement of pure β-emitters, such as highly radiotoxic ^{90}Sr, is more laborious in terms of sample preparation and measurement and therefore only a relatively small amount of samples was analysed for ^{90}Sr. The Japanese government proclaimed a maximal isotope ratio of $^{90}Sr/^{137}Cs$ of 10%. In order to ensure food safety, control measurements of ^{90}Sr in various kind of foods are needed. Therefore, in this project ^{90}Sr was isolated from the complex organic matrix with incineration and precipitation steps, followed by solid phase extraction with strontium specific resins. Thereafter, the β-activity of the isolated strontium fraction was measured using Liquid Scintillation Counting (LSC). The yield of the preparation steps was determined using the γ-emitting ^{85}Sr and exemplified a recovery of Sr ranging from 60 to 75 %. The detection limit with LSC was 40 mBq for the activity of ^{90}Sr and 20 mBq for the sum activity of ^{90}Sr and ingrown ^{90}Y. With the exception of one mushroom sample from Russia, all 37 analysed samples exhibited ^{90}Sr levels below the detection limit. Since the Russian mushroom sample did not reveal detectable ^{134}Cs levels, this contamination does not originate from Fukushima Daiichi NPP. A maximum ingestion dose was calculated based on the ^{90}Sr detection limit to be 11 µSv. The radiocesium activities of 36 samples were below the regulatory limit of 100 Bq/kg. Only one sample from Kanagawa prefecture exceeded the regulatory limit. Samples taken from within a 350 km radius around the accident at Fukushima Daiichi NPP show characteristic $^{134}Cs/^{137}Cs$ activity ratios of approx. 1 (calculated back to the time of accident). In contrast, samples from further away only show detectable ^{137}Cs activities, evidencing an origin from previous releases (primarily atmospheric nuclear explosions fallout). The worst-case effective ingestion dose from incorporated radiocesium is 28 µSv/a (^{134}Cs) and 94 µSv/a (^{137}Cs).

Keywords: Fukushima, radiostrontium, LSC, food monitioring, radiocesium

Zusammenfassung

In dieser Arbeit werden verschiedene Lebensmitteln aus Japan auf ^{90}Sr untersucht. Durch den nuklearen Unfall des Fukushima Daiichi Kernkraftwerks am 11. März 2011 wurden große Mengen an radioaktiven Substanzen unkontrolliert in die Umwelt freigesetzt. Aufgrund des Gefährdungspotentials durch die Inkorporation von Radionukliden mit der Nahrung bzw. dem Trinkwasser ist die Lebensmittelüberwachung besonders wichtig. Daher ist eine genaue und häufige Überwachung von möglicher Weise kontaminierten Lebensmitteln entscheidend. Gamma-emittierende Radionuklide wie ^{131}I, ^{134}Cs und ^{137}Cs können ohne großen Aufwand gammaspektroskopisch überwacht werden. Hingegen ist das besonders radiotoxische Nuklid ^{90}Sr als reiner Betastrahler aufgrund komplexer Probenpräparation und Messung weniger gut überwacht und wurde im Lebensmittelmonitoring nicht annähernd der gleichen Probenzahl bedacht wie Radiocäsium. Die japanische Regierung nahm anfangs ein maximales Verhältnis von $^{90}Sr/^{137}Cs$ von 10% an. Zur Gewährleistung dieses Verhältnisses und damit der Lebensmittelsicherheit sind Kontrollmessungen von ^{90}Sr in Lebensmitteln verschiedener Kategorien notwendig. Daher wurde in dieser Arbeit ^{90}Sr aus komplexer organischer Lebensmittelmatrix durch Veraschungs- und Fällungsschritte isoliert. Anschließend wurde das Strontium durch Fest-Flüssig-Extraktion mittels selektiver Strontium-Säulen weiter aufgereinigt. Die Beta-Aktivität des isolierten ^{90}Sr wurde direkt nach der Extraktion mit Hilfe von *Liquid Scintillation Counting* (LSC) bestimmt. Die chemische Ausbeute der Strontiumisolierung wurde mittels γ-emittierenden ^{85}Sr und Reinst-Germaniumdetektoren bestimmt und variierte zwischen 60 – 75 %. Die Nachweisgrenze der Aktivität beim LSC lag für ^{90}Sr bei 40 mBq und für die Gesamtaktivität von ^{90}Sr und der nachgewachsenen Tochter ^{90}Y bei 20 mBq. Mit Ausnahme einer Pilzprobe aus Russland lagen alle Proben unterhalb der ermittelten Nachweisgrenze. Die jährliche effektive Folgedosis von ^{90}Sr durch Ingestion der Lebensmittel wurde mit der spezifischen Aktivität der Nachweisgrenze und für ^{134}Cs und ^{137}Cs mit den ermittelten spezifischen Aktivitäten bestimmt. Mit Ausnahme einer Pilzprobe aus Kanagawa lagen alle untersuchten Proben unterhalb des japanischen Radiocäsium-Grenzwertes von 100 Bq/kg. In einem 350 km Radius um das Fukushima Daiichi Kernkraftwerk zeigte das $^{134}Cs/^{137}Cs$ Aktivitätsverhältnis einen für den Unfall charakteristischen Wert von 1 (zurückgerechnet zum Zeitpunkt des Unfalls). Weiter entfernte Lebensmittelproben wiesen lediglich ^{137}Cs in nachweisbaren Gehalten auf, was auf den Fallout von oberirdischen Kernwaffenexplosionen zurückgeführt werden kann.

Schlagwörter: Fukushima, Radiostrontium, LSC, Lebensmittelüberwachung, Radiocäsium

Contents

Danksagung I
Abstract II
Zusammenfassung III
1. Introduction 1
1.1. Motivation 1
1.2. Fukushima Daiichi 1
1.2.1. Nuclear power plant 1
1.2.2. Reactor type 4
1.2.3. Circumstances of the accident 7
1.2.4. Impact 8
1.3. Radionuclides and radiation exposure 10
1.3.1. Activity definition and equilibria 11
1.3.2. Radiation exposure and dose calculation 13
1.3.3. Radionuclides 16
1.4. Food safety and monitoring 19
2. Materials and methods 22
2.1. Strontium extraction chromatography 22
2.2. Liquid scintillation counting (LSC) 22
2.3. Gamma spectroscopy with semiconductors 26
2.4. Chemicals and materials 27
2.5. Instrumentation and software 28
2.6. Experiment 28
2.6.1. Sampling 28
2.6.2. Gamma spectroscopic measurement of food concentrates 29
2.6.3. Preparation of food concentrates 29
2.6.4. LSC measurement 31
2.6.5. Time dependent elution of Strontium 31
3. Results and discussion 32

3.1. Optimizing of sample preparation steps 32
3.1.1. Chemical yield determination of sample preparation 32
3.1.2. Stability of Sr resins in long-term usage 33
3.2. Evaluation of Three Window Method 33
3.2.1. Setting of the Windows and calibration curves 33
3.2.2. Determination of characteristic limits 35
3.3. Determination of ^{90}Sr in food concentrates 36
3.3.1. Test sample ^{90}Sr determination 37
3.3.2. Real sample ^{90}Sr determination 38
3.4. Gamma spectroscopic investigation of ^{134}Cs and ^{137}Cs in food concentrates 40
3.4.1. Energy calibration 40
3.4.2. Efficiency calibration 41
3.4.3. Activity determination of undisturbed discrete gamma emissions 42
3.4.4. Determination of radiosilver in food 45
3.5. Estimation of ingestion dose 46
4. Conclusion 49
5. References i
6. Appendix iv
Appendix A: List of abbreviations iv
Appendix B: List of figures vi
Appendix C: List of tables vii
Appendix D: Additional information viii
Appendix E: Certificates xi
Appendix F: Selbstständigkeitserklärung xv

1. Introduction

1.1. Motivation

This thesis is based on the events of the nuclear accident at Fukushima Daiichi Nuclear Power Plant (NPP) on March 11, 2011 in Japan and the subsequently initiated food monitoring campaign. The campaign was designed to ensure food safety of all kinds of food produced and manufactured in Japan. At the time of the accident an estimated amount of 520 PBq (noble gases excluded) of various radionuclides was released into the environment [1]. Volatile and gamma-emitting radionuclides such as ^{134}Cs, ^{137}Cs and ^{131}I were easily and constantly monitored in air, water and food [1]. To ensure food safety, about 120,000 -350,000 samples per year of various kinds of foods are still measured for their $^{134+137}$Cs activity in the prefectures close to the accident [2]. In the year of the accident 3.3% of the analysed samples in the prefecture Fukushima exceeded the provisional legal limit of 500 Bq/kg radiocesium in general foods (predominantly vegetables, fishery and animal products). In 2016 only 0.8% of the samples (Mainly mushrooms and wild animal products) were above the in April 2012 new constituted legal limit of 100 Bq/kg radiocesium [2–4]. However, the determination of radiotoxic nuclide ^{90}Sr is often scarce and few data for the overall dose estimation for humans is available [4–6]. This is due to the time-consuming preparation process of having a complex matrix separation procedure for an appropriate measurement of beta detection with Liquid Scintillation Counting (LSC) or gas ionisation detectors. Therefore, the main task of this thesis is to determine ^{90}Sr in a variety of foods, to study the correlation of ^{90}Sr/^{137}Cs and to assess the exposure to customers and the environment, resulting from anthropogenic radionuclides released in the course of the NPP accident.

1.2. Fukushima Daiichi

On the 11th of March 2011 the main island Honshū of Japan (Figure 1) was struck by an earthquake with a maximum force of 9.0 M_w, resulting in tsunami waves hitting the east coast of Japan. Due to the damage of the earthquake and tsunami, an almost complete blackout of the power supply as well as a destruction of the emergency cooling facilities of the Fukushima Daiichi NPP occurred with the result of partial core melt downs in reactor Units 1, 2 and 3 in the following days. The nuclear accident at Fukushima Daiichi NPP was classified at the highest possible nuclear accident level INES 7 by the International Nuclear and Radiological Event Scale [7]. Large amounts of radioactive substances of an estimated 520 PBq (noble gases excluded) were released into the environment due to this accident [1].

1.2.1. Nuclear power plant

Fukushima is a prefecture in the north-eastern region of the main island Honshū. The Fukushima Daiichi NPP is located at the Pacific Ocean about 60 km east of the capital

Fukushima City (Figure 1 a)). The NPP is operated by the Tokyo Electric Power Company (TEPCO) and has an overall area of 3.5 km^2. The NPP consisted of six units of light water boiling water reactors (BWRs) of type 3 to 5 with containment vessels of type Mark I and II [7]. Table 1 gives a short overview of the properties of each reactor unit. Two additional reactor units at the location were in the planning phase before the nuclear accident in March 2011. 12 km in the south of Fukushima Daiichi NPP, the Fukushima Daiini NPP is operated with four reactor units of the type BWR [7].

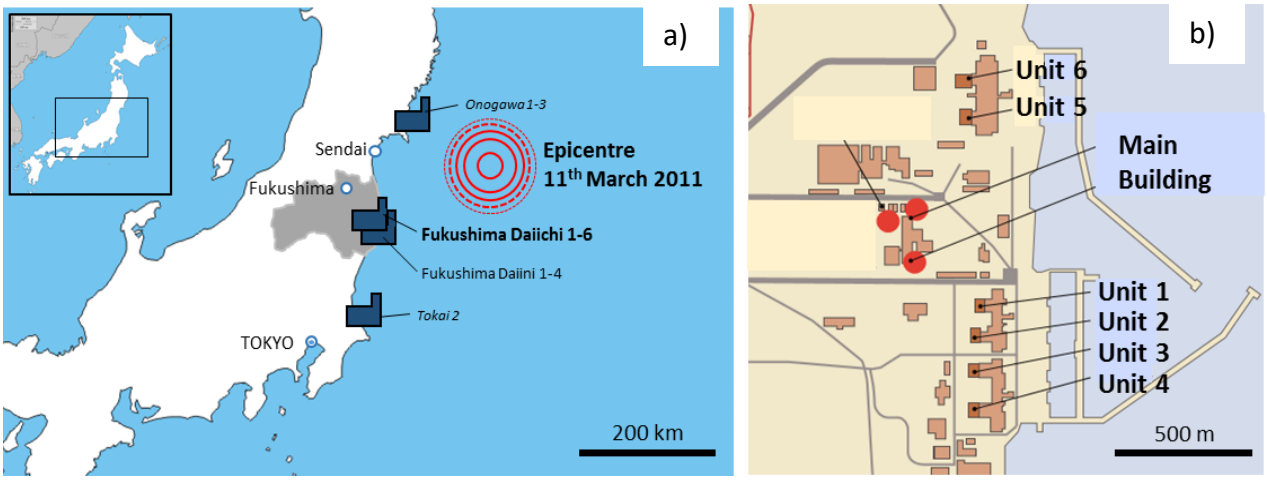

Figure 1: a) Location of the Fukushima Daiichi NPP in Japan. The grey area is the prefecture Fukushima with its capital Fukushima. The epicentre of the earthquake on the 11th March 2011 was east of the city of Sendai. b) Fukushima Daiichi NPP area with the location of the six reactor units. 1 b) modified after [7].

Table 1: Properties of the reactor units of the Fukushima Daiichi NPP [7].

Unit	Type	Containment	Date of commercial operation	Electric power [MW]	End of operation
1	BWR 3	Mark I	1971	460	2011
2	BWR 4	Mark I	1974	784	2011
3	BWR 4	Mark I	1976	784	2011
4	BWR 5	Mark I	1978	784	2011
5	BWR 5	Mark I	1978	784	2014
6	BWR 5	Mark II	1979	1100	2014

A cross section of Unit 1 is shown in Figure 2 [7]. Every reactor building has an own cooling pool for spent fuel rods. At Units 1-4, the power house is connected directly to the reactor building and lies towards the sea side at a sea level of about 10 m. The power house holds the steam

turbine with power generator, diesel emergency power generator and emergency batteries. At Unit 1, both diesel emergency power generators are in the power house to the seaside. At Unit 2-4, one emergency diesel backup generator was located in the power house and the other generator facing the main reactor building inland. For cooling purposes, seawater was transported from the Pacific Ocean towards the power house. The tsunami protection wall was 5.7 m tall, whereby the height was calculated from the worst tsunamis in the recent 100 years. The tsunami wave height resulting from the earthquake on the 11th of March 2011 exceeded the calculation by far with up to 14 m height.

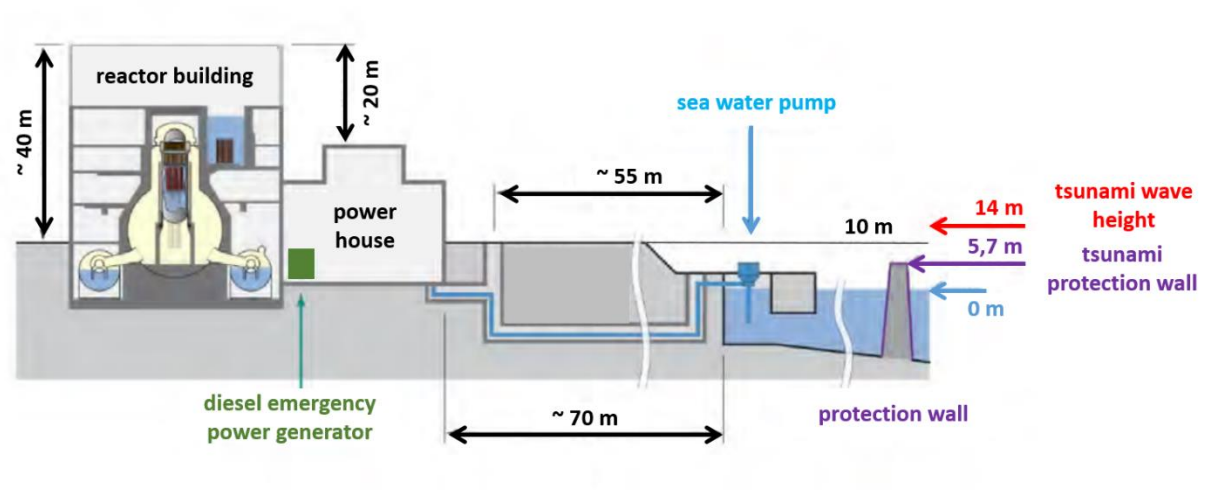

Figure 2: Profile of Daiichi NPP Unit 1 with the reactor building directed inland and with the affiliated power house towards the sea. The height of the tsunami wave and the height of the protection wall are indicated. Modified after [7].

The reactor Units 5 and 6 are about 100 m north from Unit 1 at a natural plateau and were not directly hit by the tsunami. Furthermore, the power plant has a separate holding basin and a dry storage tank for new and used fuel rods. At the day of accident, the used fuel consisted of low enriched uranium dioxide UO_2 with the exception of reactor unit 3, which contained 32 fuel assemblies with mixed oxides (MOX) with 3-10 % plutonium dioxide PuO_2 and 516 fuel assemblies of low enriched uranium (LEU) [8]. The exact amounts of nuclear fuel inside the units are presented in Table 2. Overall, about 14700 fuel rods with a weight of 2500 tons of new and spent fuel rods were at the plant on the 11th of March 2011 [9]. Each reactor core used control rods consisting of B_4C/Hf [7].

Table 2: Amount of fuel inside the units at the time of accident on the 11th of March 2011 [7, 9].

Unit	Fuel material [7]	Reactor fuel assemblies [7]	Spent fuel assemblies [9]	New fuel assemblies[9]
1	UO_2	400	392	100
2	UO_2	548	615	28
3	UO_2/MOX	548	556	52
4	UO_2	0	1535	204
5	UO_2	548	994	48
6	UO_2	764	940	64
Central Storage	UO_2		6375	

1.2.2. Reactor type

Fukushima Daiichi NPP consisted of 6 reactors of the type light-water boiling reactor (BWR) 3-5 with containments of MARK I (Units 1-5) und MARK II (Unit 6) [7].

A reactor has two parts: the reactor building with the reactor core and the neighbouring power house to generate the energy. The reactor building consists of the reactor pressure vessel (RPV) holding the reactor core with the nuclear fuel inside. Control rods are located at the bottom of the RPV at BWRs and can be inserted from the bottom into the reactor core. Several recirculation pumps are connected towards the RPV. The RPV is filled above the reactor core with demineralized water. The demineralized water serves as coolant and neutron moderator by surrounding the fuel assemblies. The heat produced by fission inside the fuel boils the surrounding water and the steam is transported through pipes towards the power house. Inside of the power house, the produced steam is transported to the turbines, which drives an electric generator. Parts of the produced energy are used for self-sustaining energy for a diversity of pumps and electrics and the remaining energy is transformed for the external energy grid. Thereafter, the steam is subsequently cooled by a sea water cooling condenser and pumped back into the RPV.

The lower parts of reactor building are made of reinforced concrete to protect it against external impacts and the upper part is made of steel. At the BWRs at Fukushima Daiichi, the spent fuel pool is located inside the upper reactor building with a fuel removal crane. The used fuel rods spent about 3 to 5 years after removal from the core inside the spent fuel pool. The reactor pressure vessel has an approximate height of 20 m and is located in the centre in the reactor building. Each reactor core (height: approx. 3.5 m) can hold a specific amount of fuel assemblies (Unit 1: 400, Units 2-5: 548; Unit 6: 764). The RPV is made of 16 cm thick steel with several openings. For radiation protection and accident prevention reasons, the RPV is

surrounded by a containment. The primary containment vessel (PCR) consists of a drywell and a condensation chamber. The drywell of the type MARK I has the shape of an inverted lightbulb and the bottom is surrounded by a steel torus, the condensation chamber. The drywell contains a biological shield around the reactor core. The torus-shaped condensation chamber is located below the sea level and is partly filled with water. Upon emergency shutdown and loss of external cooling, the condensation chamber is designed to condensate steam from inside the RPV and to provide the RPV with an (limited) amount of cooling water. The whole primary containment is filled with nitrogen, to avoid the onset of explosive oxy-hydrogen gas during incidents. The PCR is enclosed by the secondary containment building, which has a slightly lower pressure than atmosphere to keep possible volatile radioactive materials inside the reactor building [7].

The power supply of the power plant is covered during operation by the energy generated at the power plant. If the plant ceases operation, the energy is taken from the external electrical grid. For emergency situation – in the case that no external power supply is available – two separate diesel emergency power generators are assigned for each unit. Each diesel emergency power aggregate can generate 100% of the energy needed to cool the reactor. At complete station blackouts, when not even the emergency aggregates can produce energy, emergency batteries can supply energy for the following 10 hours after station blackout [7].

The reactor core is in need of constant cooling during operations and after emergency shutdowns because of residual heat. Therefore, several cooling systems for regular operations and in case of emergencies are installed. During regular operation the steam is cooled by a condenser in the power house and pumped back into the RPV to keep the filling level of the water. After a reactor emergency shutdown, it remains necessary to cool the reactor core continuously due to the residual heat. The residual heat is produced by the delayed beta decay of the fission products and is about 6.5% of the original thermal core power right after shutdown. After one hour, the residual heat is about 1.6% of the original core power and therefore still produces several MW of power. The cold shutdown is declared after the core reaches a temperature below 100 °C at atmospheric pressure. The thermal power of the residual heat depends on the type of fission products and their half-lives. The failing of heat removal results in core heating and possible structural damage to the core (core meltdown). Furthermore, the spent fuel rods are as well in need of steady cooling at the spent fuel pool due to various radionuclides present in the nuclear waste [10, 11].

In case of emergency several redundant and diverse cooling systems are available, which are operable with different power sources [7]:

1. The **residual heat cooling system** works by cooling the coolant of the RPV in a heat exchanger with sea water. For the operation of residual heat cooling system electric

high pressure coolant injection pumps are necessary, which energy can be generated by emergency diesel aggregates.

2. The **Residual Heat Removal System** (RHR) functions only at low pressure in the RPV. During regular operation, it is used for cooling of the residual heat through a heat exchanger and pumping the coolant back into RPV. In case of emergencies, the water coolant can be taken from the condensations chamber and can then be cooled with the heat exchanger. Afterwards the coolant can be sprayed back into the RPV.
3. The **Isolation Condensor** (IC) is used for lowering the pressure and temperature by condensation of the steam from RPV in pipes with outer water reservoirs. The steam condensates in the pipes and flows back into the RPV. The IC does not need electrical pumps and can be operated by opening of valves from the RPV with a DC battery even at station blackout. The IC can cool the steam of the residual heat up to 8 hours after shutdown.
4. **Emergency Core Cooling System** (ECCS) consists of two independent systems: the high-pressure coolant injection system (HPCI) and the Core Spray system (CS). The HPCI allows the injection of coolant into RPV at high pressures with a pump operated by a turbine driven by the steam of the RPV. Hereby the steam flows to the pressure suppression chamber and drives the local turbine. The coolant can be taken from condensation chamber. The CS can inject coolant at low pressures in the RPV. The water can be taken from the condensation chamber with electric pumps.
5. The **Containment Cooling System** (CCS) allows heat removal from the containment and the condensation chamber by a heat exchanger. Afterwards the coolant can be reinjected into the condensation chamber by electrical pumps.
6. The **Reactor Core Isolation Cooling System** (RCIC) pumps the coolant into RPV to keep the filling level. The pumps take the water from the condensation chamber and can spray the coolant even at high pressure back into the RVP. The pumps can be operated with DC power from batteries.

Unit 1 has a reactor shutdown cooling system, IC, ECCS and CCS. Units 2-4 are equipped with RHR, ECCS and RCIC [7].

The RPV and the containment have design pressure limits. At higher pressures (e.g. due to rising temperatures) risk of damages of the used building materials arise. Furthermore, only some parts of the several coolant systems are functional at higher pressures. When reaching the pressure limit in the RPV, pneumatic valves towards the condensation chamber open. Thus, the temperature and the pressure rises inside the containment vessel. To avoid damages of the containment at continuously rising pressure (as in case of failing cooling of the residual heat), venting of the containment over the stack is a possible option. Venting describes the process of controlled but unfiltered release of the steam (possibly containing radioactive substances)

inside the containment into the environment. The power of a DC Battery is necessary for the venting process to open the valves towards the exhaust gas stack. At Fukushima Daiichi NPP Units 1 & 2 and Units 3 & 4 share one exhaust gas stack [7].

The accident occurred due to the failing of the cooling of the decay heat in the reactors after scram. Due to lack of contact between fuel and coolant water, local heating of the reactor fuel takes place. At reaching a temperature of 900 °C the fuel begins to oxidise and fuel cladding tubes burst. In this process, a fraction of fission products and most of the noble gases are released. The continuous heating of the fuel and the inserted control rods leads to the destruction and melting of the control rods. In case of the BWR control rods of eutectic steel with boron carbide and hafnium are destroyed above 1400 °C. Furthermore, hydrogen is produced by the reaction of steam with the zirconium alloy cladding tubes ($Zr + 2\ H_2O \rightarrow ZrO_2 + 2\ H_2$). With temperatures in excess of 2000°C, the fuel cladding tube is further oxidised and the tube and fuel rods start melting, resulting in high releases of fission products. Afterwards, the melted fuel can flows downwards and may damage the reactor pressure vessel and possibly the containment. A damaged RPV and PCR can lead to uncontrolled release of radionuclides into the environment [7].

1.2.3. Circumstances of the accident

At the time of the accident Units 1, 2 and 3 were in regular operation, whereas Units 4, 5 and 6 were under revision. In Unit 4, all fuel rods (1331 spent fuel rods and 204 new fuel rods) were in the spent fuel pool. In Units 5 and 6, the fuel cores were inside the RPV. At Unit 5, pressure tests were conducted at the time of accident and Unit 6 RPV was depressurized [7].

Units 1 - 3 showed similar accident scenarios, only differing in time intervals. After the tsunami hit, a total power failure occurred, resulting in loss of several regular and emergency cooling functions. Due to decay heat, the temperature and pressure rose inside the RPV, producing high amounts of steam and leading to a decline of cooling water level. The decreasing water level left the fuel uncovered by water; the core was damaged and started melting with increasing temperatures. At these high temperatures, water reacts with the core cladding tube material and hydrogen is produced. The hydrogen and radioactive materials containing steam leaked through the damaged RPV and Primary Containment Vessel and accumulated inside the reactor building. Through reaction of highly concentrated hydrogen with natural oxygen, hydrogen explosion destroyed the reactor building in Units 1, 3 and 4. The hydrogen concentration in Unit 2 did not reach the explosion limit, because of a blown-out panel at the reactor building. The hydrogen for the explosion in Unit 4 flowed from the venting process of Unit 3 through the exhaust pipes for the stack into Unit 4 [7, 12].

1.2.4. Impact

The environmental impact of a nuclear event is classified by the International Nuclear and Radiological Event Scale (INES) initiated by the International Atomic Energy Agency (IAEA) to ensure an easy and fast transnational grading of events involving nuclear power. The INES diagram (Figure 3) shows the rating of levels from 0 – 7. Level 0 events have no safety relevance or significance, level 1-3 are nuclear incidents and level 4 - 7 are defined as nuclear accidents. The highest event level 7 is defined as major releases of radioactive substances into the environment with widespread health and environmental risks. Only two major accidents, namely the Chernobyl Unit 4 accident and the accident at Fukushima Daiichi involving four units were declared as INES level 7. Each unit of Fukushima Daiichi NPP was rated independently: Unit 1-3 with partial core melt downs as INES level 5 with releases of several percentages of the core inventory and Unit 4 due to heating of the spent fuel as a serious incident of INES level 3 [7, 13].

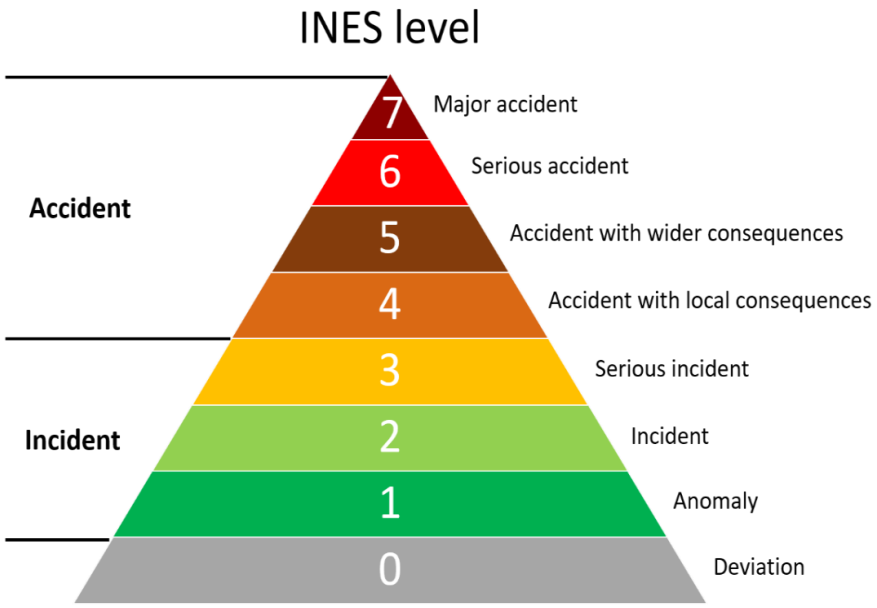

Figure 3: The rating system of the international nuclear and radiological event scale (INES).

The releases of radionuclides into the environment from Units 1-4 resulted from the damage of the RPV due to insufficient cooling of the core and a following core melt down. In this process the primary containment vessel and the reactor building were damage by high pressures and hydrogen explosion leading to a continuous release of radionuclides. Most emissions were produced by Units 1 – 3 and only small amounts of radionuclides were released by the spent fuel pool of Unit 4. Current publication show that most releases originated from Unit 2, possibly due to severe damage of the RPV and containment. Both Unit 5 and 6 could be further cooled at time of accident, therefore no significant emissions were released from these reactors.

Through venting and hydrogen explosions especially volatile radionuclides as noble gases, iodine and cesium were released into the environment [13].

The activity of the overall released radionuclides – except the noble gases – during the Fukushima Daiichi accident is estimated to be maximal 520 PBq [1]. In contrast 5200 PBq was released during the Chernobyl disaster [14]. Estimated atmospheric releases are about 0.3 - 6% of the core inventory of radiocesium, more specifically around 11.8 PBq ^{134}Cs and 12 PBq of ^{137}Cs [1]. Furthermore, 160 PBq of radioiodine and 0.14 PBq of ^{90}Sr and 2 PBq of ^{89}Sr were released from the Fukushima Daiichi NPP accident [13].

In addition to the atmospheric releases, radionuclides were also released into the environment dissolved in water. At some point contaminated water leaked from the PCR in Units 1-3 and accumulated at the bottom of the reactor building. Furthermore, some amounts of the leaked steam from the containment was washed out by external cooling water supply and rain, and accumulated as well in the reactor building. The accumulated contaminated water inside the reactor building leaked to some parts into the power house through different valves and connections. Thereafter some parts of the contaminated water could leak directly into the sea. Overall about 90000 m^3 contaminated water accumulated in the Unit 1 – 4. The activity concentration inside the power house was 0.13 GBq/L – 3 GBq/L for ^{137}Cs and 0.15 GBq/L – 13 GBq/L for ^{131}I. Especially Unit 2 showed a contamination in the power house water one magnitude higher than Units 1 and 3, probably due to a leaking torus. It is estimated that 4.7 PBq of contaminated water was directly released into the sea by various events. Through a leakage 520 m^3 and 250 m^3 highly contaminated water from Unit 2 and 3 were released, respectively. Additionally, 9070 m^3 of low contaminated water from Units 1-4 and 1320 m^3 of low contaminated water from Units 5 and 6 were deliberately released because of missing storing capabilities on the plant area [13]. Since June 2011, the remaining contaminated water sources are step for step decontaminated and stored in tanks on the plant area [12].

For regular monitoring of ambient dose rates, some permanently installed measuring stations had been installed on the nuclear power plant site. Due to the earthquake and tsunami most permanently installed measuring stations were severely damaged and replaced by mobile measuring station for radiation monitoring after the nuclear accident around the area of the power plant. Local maxima of the ambient dose rate at the power plant originated at major events after the release of radionuclides during hydrogen explosions and venting processes. In this nuclear event, ambient dose rates up to 12 mSv/h have been measured at the border of the area of the NPP. The ambient dose is continuously decreasing since April 2011, but local hot spots from contaminated debris have been registered since, making a decontamination necessary before clean-up operations [13].

The plume containing radioactive material was mostly blown offshore over the Pacific Ocean. However, on the 15th/16th of March, a large amount of radionuclides was distributed on the Japanese mainland mass in north-western region several kilometres from the NPP (cf. radiocesium deposits from Fukushima Daiichi NPP accident in Figure 4 [13]). For radiation protection reasons, exclusion zones around the Fukushima Daiichi NPP were established. 20 km around the plant were declared as restricted area. The entry in the restricted area is prohibited for all with exception of work force and temporary by municipalities allowed persons. Between the 20 km and 30 km radius around the plant an evacuation-prepared area in case of emergency was established. This area is recommended to leave voluntary, furthermore only controlled and restricted life is possible. Due to the north-western plume, a deliberate evacuation area in the north-west was established. The effective dose in the first year after the accident in the deliberate evacuation zone is estimated to be above 20 mSv/a and for this reason the population is requested to leave [13].

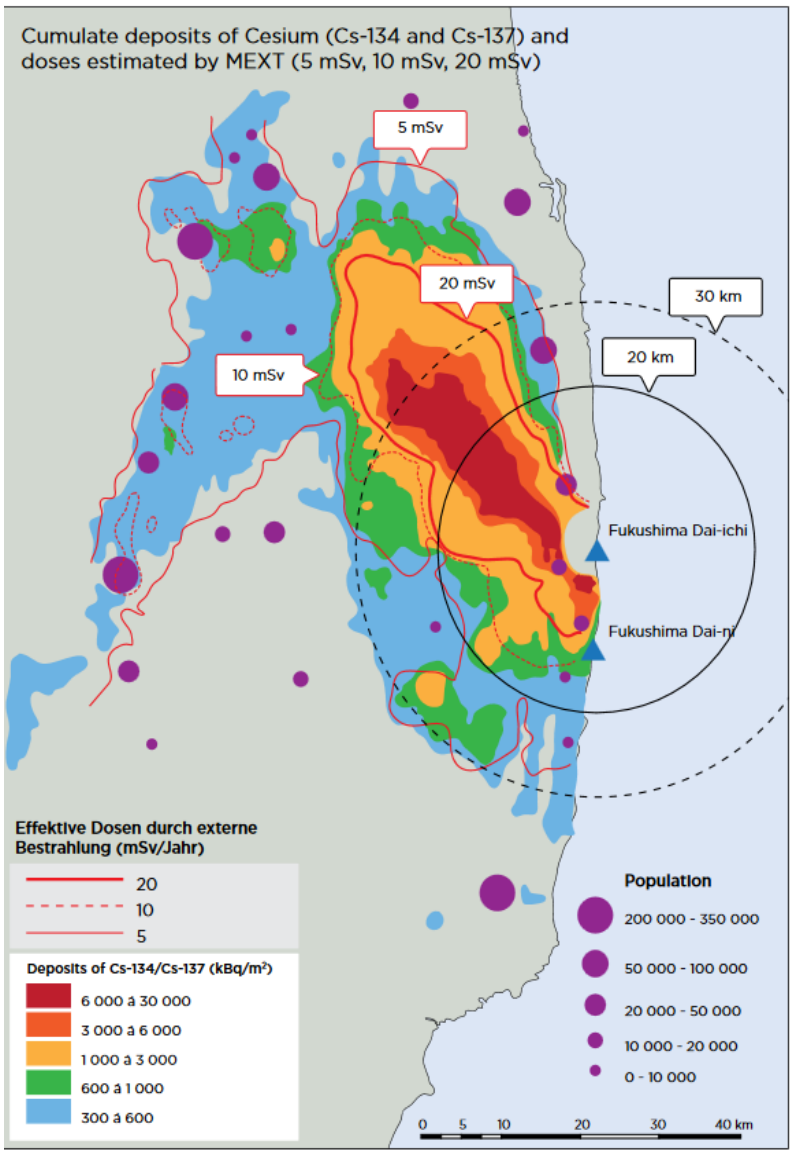

Figure 4: Deposits of cumulated cesium activity released during Fukushima Daiichi NPP nuclear accident. Estimated effective doses from external radiation from specific regions are labelled with red lines [13]

1.3. Radionuclides and radiation exposure

Radioecology describes the science of production, existence and distribution of radionuclides in the environment. The main task of radioecology is the analysis of natural and anthropogenic radionuclides in respect to its behaviour in environment and potential risk management for the

human kind. In this aspect, especially food safety is of high importance for health issues and therefore needs to be controlled on regular base.

1.3.1. Activity definition and equilibria

The activity *A* is defined as the frequency of transitions of instable nuclear conditions (nucleus disintegrations) and can be described as sum of decay rate λ and quantity of the nucleus $N(t)$ at time *t* (Eq. 1.1). The SI unit for the activity is Becquerel Bq = s^{-1}.

$$A = \frac{\text{Disintegration}}{\text{Time}} = -\frac{\mathrm{d}N(t)}{\mathrm{d}t} = \lambda \cdot N(t) \tag{1.1}$$

The differential equation of the activity (Eq. 1.1) can be mathematically integrated, resulting in the decay law (Eq. 1.2). N_0 is the initial quantity of the nuclei. The equation is only sufficiently precise for large quantities and macroscopic time intervals.

$$N(t) = N_0 \cdot e^{-\lambda t} \tag{1.2}$$

The decay rate λ is correlated to the inverse mean lifetime τ and half-life $t_{1/2}$ (Eq. 1.3). The decay rate is specific for every transition. Half-live $t_{1/2}$ describes the time necessary to decay to half of the initial quantity of nuclei.

$$\lambda = \frac{1}{\tau} = \frac{\ln(2)}{t_{1/2}} \tag{1.3}$$

If the decay product is an instable nucleus as well, the activity of the daughter nuclide needs to be considered in activity calculations. The parent-daughter relationship can be described as the following equation 1.4 with X_P being the parent radionuclide, X_D the radioactive daughter nuclide and *Y* the stable decay product.

$$X_P \xrightarrow{\lambda_P} X_D \xrightarrow{\lambda_D} Y \tag{1.4}$$

The quantity of the daughter radionuclide N_D is calculated by the production rate of the daughter nuclide (equals the decayed quantity of the parent nuclide) and the decay of the daughter nuclide, and can be described with the equation 1.5.

$$\frac{\mathrm{d}N_D}{\mathrm{d}t} = -\frac{\mathrm{d}N_P}{\mathrm{d}t} - \lambda_D \cdot N_D = \lambda_P \cdot N_P - \lambda_D \cdot N_D \tag{1.5}$$

Through solving the differential equation of Eq. 1.5, under the condition that at time $t = 0$ no atoms of the daughter nuclides are present, the following Eq. 1.6 is formed.

$$N_D = \frac{\lambda_P}{\lambda_P - \lambda_D} \cdot N_P \cdot \left(1 - e^{-(\lambda_D - \lambda_P)t}\right) \tag{1.6}$$

After reaching the equilibrium the exponential function of equation 1.6 is zero and the radioactive equilibrium can be described with equation 1.7. The time needed to attain the radioactive equilibrium depends on the half-lives of the parent and daughter nuclide.

$$N_{\mathrm{D}} = \frac{\lambda_{\mathrm{P}}}{\lambda_{\mathrm{P}} - \lambda_{\mathrm{D}}} \cdot N_{\mathrm{P}} \tag{1.7}$$

As a consequence of the parent-daughter relationship (Eq. 1.4) and their decay rate, three different types of equilibria can be differentiated: secular equilibrium, transient equilibrium and no equilibrium with following boundary conditions.

1. secular radioactive equilibrium: $\lambda_P \ll \lambda_D \leftrightarrow t_{1/2,P} \gg t_{1/2,D}$ (1.8)

Taking the high differences of the decay rate of parent and daughter nuclide into account, the decay rate of the mother is negligibly small; it does not need to be considered in the equation 1.6 which simplifies the activity equation 1.9 for secular equilibria.

$$N_{\mathrm{D}} = \frac{\lambda_{\mathrm{P}}}{\lambda_{\mathrm{D}}} N_{\mathrm{P}}\left(1 - e^{-\lambda_{\mathrm{D}} \cdot t}\right) \tag{1.9}$$

The activity of the daughter nuclide $A_{\mathrm{D}}(t)$ approximates after several half-lives to the activity of the parent nuclide $A_{\mathrm{P}}(t)$ and reaches the equilibrium after about 8 half-lives with nearly 99 % activity ratio and the equation 1.10 applies.

$$A_{\mathrm{D}}(t) = A_{\mathrm{P}}(t) \tag{1.10}$$

The ingrowth of the daughter nuclide is shown for the example of ^{90}Sr in Figure 5. The ingrowth speed is at the beginning fast and decreases with time.

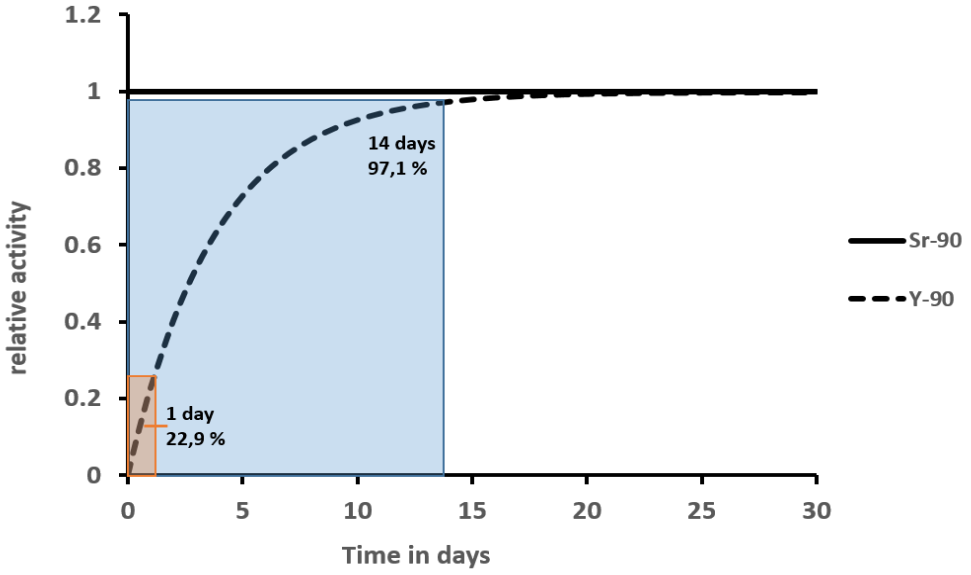

Figure 5: secular equilibrium of ^{90}Sr with ingrowing daughter nuclide ^{90}Y.

2. transient radioactive equilibrium: $\lambda_P < \lambda_D \leftrightarrow t_{1/2,P} > t_{1/2,D}$ (1.11)

In case that the half-life of the daughter nuclide is not negligible in respect to the half-life of the parent nuclide a transient equilibrium adjusts after various half-lives. The activity of the

daughter nuclide is always higher by a constant factor than the activity of the parent nuclide in a transient equilibrium.

3. no radioactive equilibrium: $\lambda_P > \lambda_D \leftrightarrow t_{1/2,P} < t_{1/2,D}$ (1.12)

When the half-live of the parent nuclide is lower than the half-live of the daughter nuclide, the activity ratio never reaches equilibrium and consequently changes until the parent nuclide is completely decayed [15, 16].

1.3.2. Radiation exposure and dose calculation

The environment and humans are constantly exposed to ionizing radiation from cosmic radiation as well as from radionuclides with natural or anthropogenic origin. The radiation exposure is differentiated in external and internal exposure to ionizing radiation. For the external radiation exposure, mostly γ-rays are considered for calculation of effective doses. The β- and α- radiation only have a relatively short range in air and notably within solid matter and can be easily shielded. Therefore the dose for external exposure – resulting β- and α-radiation – needs to be particularly considered for skin dose at close distances. However, for internal exposure α, β und γ radiation are of importance for dose calculations. Internal exposure occurs by incorporation of radionuclides. The incorporation takes place by inhalation of gaseous substances or dust particles or by ingestion of drinking water or food. Especially α-radiation has a high impact on the resulting effective dose by incorporation because of high energy transfer to the surrounding tissue [15].

Through the uptake of food the human body incorporates necessary nutrition and trace elements, but also pollutants. Depending on the chemical properties of the pollutant, a bioaccumulation in specific biological tissue is possible. From a radio ecological perspective, the incorporation of radionuclides involves a risk for damaging sensible tissue, due to their high energy transfer. Particularly, when the radionuclide is accumulated in tissue and has a longer time (until the excretion or decay) for interaction with the surrounding matter. Therefore, an evaluation of the potential risk needs to consider several aspects as radiological half-life, biological half-life, and type of radiation and energy of the ionizing radiation. Hence, the following equations are used for radiation protection and dosimetry [15].

The absorbed dose $D_{T,R}$ describes the absorbed energy of the radiation (α,β,γ,n,…) to a specific mass of tissue T (Eq. 1.13). The unit for the absorbed dose is Gray (Gy = J·kg^{-1}).

$$D_{T,R} = \frac{\text{transferred energy of radiation } R}{\text{mass of tissue } T} \quad [\text{Gy} = \text{J}\cdot\text{kg}^{-1}] \tag{1.13}$$

The equivalent dose H_T takes the different biological effect of different types of radiation towards tissue into consideration with the radiation weighting factor w_R (Eq. 1.14). The weighting factor for x-rays and gamma rays as well as beta rays is 1, for protons with energy

higher than 2 MeV 5 and for alpha rays and nuclear fission products 20. The weighting factor for neutrons depends on their energy (<10 keV: 5; 10 -100 keV: 10; > 0.1 -2 MeV: 20; >2 – 20 MeV: 10; >20 MeV: 5). For the equivalent dose Sievert (Sv = J·kg^{-1}) is used as unit.

$$H_T = w_R \cdot D_{T,R} \quad [\mathrm{Sv} = \mathrm{J} \cdot \mathrm{kg}^{-1}] \tag{1.14}$$

Furthermore, the effective dose *E* takes the different sensitivities of every tissue towards radiation into account with the specific weighting factor for every tissue w_T (Eq. 1.15). Especially, red bone marrow, colon, lung, stomach and breast have a high sensitivity towards radiation and therefore high weighting factors with each 0.12. Whereby, relativity insensitive tissues as skin and bone surface have only weighting factors of 0.01. The unit is the same as for the equivalent dose with Sievert Sv.

$$E = \sum_T w_T \sum_R w_R \cdot D_{T,R} \quad [\mathrm{Sv} = \mathrm{J} \cdot \mathrm{kg}^{-1}] \tag{1.15}$$

The effective dose by ingestion of food and drinking water E_{ing} can be described with the following equation 1.16. It considers the sum of the activity concentration $A_{\mathrm{m,r}}$ of different ingested radionuclides *r*, the annual food consumption $\dot{U}$, the time of exposure t_{exp} and the dose coefficient $g_{\mathrm{ing,r}}$ for different radionuclides *r*. The regional specific food consumption and the dose coefficient can be taken from literature. The unit is Sv·a^{-1}.

$$E_{\mathrm{ing}} = \sum_r A_{\mathrm{m,r}} \cdot \dot{U} \cdot t_{\mathrm{exp}} \cdot g_{\mathrm{ing,r}} \tag{1.16}$$

The mean annual effective dose from natural radiation for an adult in Germany is 2.1 mSv and in Japan 1.6 mSv, consisting of cosmic radiation, terrestrial radiation, internal radiation and inhalation of radon and its decay products. Additionally, the human is exposed to anthropogenic radiation. Thereby, the exposure from medical application has the highest impact on the effective dose (e.g. whole-body computer tomography: 20 mSv per application). Other anthropogenic sources are fallout radiation and nuclear power plants. The average annual effective dose in Germany resulting from nuclear power plants is 10 µSv. Through nuclear accidents – like Fukushima and Chernobyl – an uncontrolled release of high amounts of radioactive substances into the environment is possible. The nuclear fallout of the disaster can cause increased effective dose at certain areas and therefore the admission is restricted by law (e.g. 30 km radius around Fukushima Daiichi NPP: up to additional 20 mSv/a for radiocesium [7]) [17].

Ionizing radiation can induce deterministic or stochastic damage to the organism. Deterministic damage has a threshold limit – at this limit visible damage such as erythema occurs. The higher the received dose the higher the radiation caused damages, with doses > 5 Sv causing death in the following days of exposure. On the contrary, stochastic damage does not have a threshold

and the possibility of the appearance of damage ascends with higher doses. One example for stochastic damage is cancer, which often cannot be clearly associated with radiation level impact, because of statistically occurrences of cancer [15, 17].

1.3.2.1 Natural radiation exposure

In nature several natural occurring radionuclides can be found. The origin of these radionuclides is diverse: terrestrial, cosmic and anthropogenic radionuclides. Anthropogenic radionuclides are described closer at chapter 1.3.2.2 Man-made radiation exposure.

Cosmic radiation consists of galactically and solar radiation, which produces primary high energy protons. These protons can interact with the atoms of the atmosphere and produce secondary radiation as photons, protons, electrons, muons and neutrons. Some of this radiation is shielded by the atmosphere and does not reach the surface of the earth. The cosmic radiation exposure is about 0.3 mSv/a (sea level) annually. The cosmic radiation depends on the eleven year cycles of the sun [18].

Terrestrial radiation is produced mostly by primordial radionuclides and their decay products. Primordial radionuclides exist since the birth of the universe and still exist in measureable concentration on earth due to their very long half-lives. The primordial isotope ^{40}K ($t_{1/2} = 1.3 \cdot 10^9$ a) is accumulated in animals by ingestion and is the highest natural radiation exposure in humans. Other primordial radionuclides are ^{238}U, ^{235}U and ^{232}Th and their decay series. The ^{237}Np decay series is extinct due to its relatively low half-life. The decay daughter nuclides of the still existing decay series have varying half-lives until the reach to stable lead isotopes. In case of no disruption of the decay series, all daughter nuclides are present in secular equilibrium with their parent nuclide. One of the dominant radionuclides for incorporation effective dose is the noble gas radon (^{222}Rn, ^{220}Rn and ^{219}Rn) because if its gaseous state and short half-life. The alpha emitting radon makes up more than half of the annual effective dose through inhalation [18].

1.3.2.2 Man-made radiation exposure

Additionally to natural radiation, humans are exposed to anthropogenic radiation from different kind of sources. The highest anthropogenic radiation exposure results from medical diagnostic therapies as x-Ray diagnostics. The average adult effective dose in Germany from medical use is 2 mSv/a. However, the dose is highly dependent on each individual medical treatment.

Moreover, the background radiation resulting from atmospheric nuclear weapon test increased in the 50 - 60th and decreases along with the half-lives of the globally deposited radionuclides. Due to low mixing of the air in the northern hemisphere and southern hemisphere, the radiation exposure is higher on the northern hemisphere, where most nuclear weapon tests were carried out. Furthermore, nuclear power plants and reprocessing plants for spent nuclear

fuel have as well an impact on the anthropogenic radiation exposure. Around 0.01 mSv/a effective dose from normal operated nuclear power plants are received in Germany [17].

The radionuclides, which are produced and released by nuclear fission, are highly dependent on the fission product yield of the fuel material. The fission products are the fragments of the split heavy nucleus. Normally two medium heavy fission products are produced by an asymmetrical splitting of the heavy nucleus. The heavy nucleus splits asymmetrically into two maxima close to the magic numbers (mass regions around 95 and 135) for stability reasons. The percentage of yield sums up to 200 % in regards to the splitting nucleus. The resulting fission yield curves depend on the heavy nucleus (^{235}U and ^{239}Pu) and the energy of the neutrons (thermal, fast) inducing the fission. The direct fission products are instable and have a high excess of neutrons as the original nucleus and therefore produce some small amounts of delayed neutrons. The produced unstable fission product nuclei decay with β^- processes towards stable nuclides, some radiological important medium- and long-lived products and their yields from nuclear fission are presented in Table 3. [19]

Table 3: Medium and long lived fission product yields for most commonly used ^{235}U and ^{239}Pu with fission inducing thermal neutron [19].

Fission product	Half-life [20]	Yield from ^{235}U in % [19]	Yield from ^{239}Pu in % [19]
^{90}Sr	28.87 a	5.73	2.01
^{131}I	8.025 d	2.88	3.72
^{134}Cs	2.07 a	$1.21 \cdot 10^{-7}$	$6.7 \cdot 10^{-4}$
^{137}Cs	30.07 a	6.22	6.59
^{99}Tc	211,100 a	6.13	6.18
^{129}I	15,700,000 a	0.71	1.41
^{135}Cs	2,300,000 a	6.61	7.36

1.3.3. Radionuclides

The released radionuclides by nuclear accidents often vary strongly by the circumstances of the accident emissions. The released radioactive materials are in the form of fuel particles, fission and activation products. These radionuclides differ with their nuclear characteristics with every isotope and biological efficiency with every element. Primarily, fission and activation products as ^{134}Cs, ^{137}Cs, ^{131}I, ^{3}H, ^{89}Sr and ^{90}Sr are determined and evaluated.

1.3.3.1 Radiostrontium

Strontium is an alkaline earth metal with an abundance of 0.014 % in the earth's crust. Strontium exhibits chemical similarity to its lighter alkaline earth metal homologue calcium. Both can be found in nature mostly in the mineral form of carbonates and sulfates, whereas

strontium has a slightly lower solubility product constant than calcium. The only relevant oxidation state of alkaline earth ions is +II. Strontium has four stable isotopes. : ^{84}Sr (0.56 %), ^{86}Sr (9.86%), ^{87}Sr (7 %), ^{88}Sr (85.58 %) and 26 radioactive isotopes consisting of β^- and β^+ emitters [21].

Strontium is of no biological necessity for humans, but due to its similar physical and chemical properties to calcium (calcium-analogue), it is actively incorporated by the organism. The incorporation of strontium is mainly as Sr-Apatite ($Ca,Sr_3(PO_4)_2 \cdot Ca,Sr(F,Cl,OH)_2$) in teeth and bone structures. The biological half-life of strontium depends on the individual (age, height, food consumption and region) and varies between 3 – 20 a [21, 22]. Due to the close distances of incorporated strontium towards sensible tissue as bone marrow, beta emitting radiostrontium can permanently damage the tissue, resulting in higher possibility in developing cancer [5].

The decay scheme of **^{90}Sr** (Figure 6) shows the following daughter nuclides by β^- decay until the stable ^{90}Zr. ^{90}Sr is a pure beta emitter and decays to ^{90}Y with a half-life of 28.76 a and a beta endpoint energy of 546 keV. The daughter radionuclide ^{90}Y has a relatively short half-life of 64 h and forms a secular equilibrium with ^{90}Sr. At 14 days, the activity of ^{90}Y reaches 97 % of the initial activity of the parent nuclide ^{90}Sr. Therefore the activity of ^{90}Y can be used to determine the activity of ^{90}Sr and thus often used in radiochemical analysis. ^{90}Y undergoes a β^- decay to ^{90}Zr with a probability of 99.99 %. The chance of the emission of a γ quant is less than 10^{-6} %, which obstructs gamma measurements [20]. The stable ^{90}Zr has a natural abundance of 51.45 %. Due to it high natural abundance, mass spectrometric methods for determination of ^{90}Sr are challenging to be used because of isobaric interferences. To avoid isobaric interferences, collision cells with oxygen for the formation of ZrO_2 with a different initial mass can be used as shown in [23].

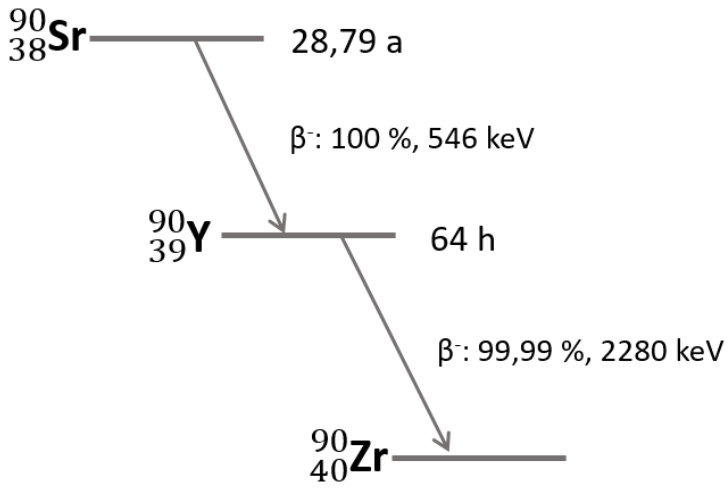

Figure 6: ^{90}Sr decay scheme. ^{90}Sr is a pure emitter with a half time of 28.79 a and decays to ^{90}Y. Due to the short half time of ^{90}Y (64 h), the parent and daughter radionuclide form a sequiliar equilibrium. ^{90}Y decay into the stable ^{90}Zr.

The major environmental inputs of ^{90}Sr are in consequences of atmospheric nuclear weapon explosions of the 1950/60s, with a considerably release of up to $8.3 \cdot 10^{17}$ Bq ^{90}Sr activity [22]. Furthermore, ^{90}Sr was released into the environment in the course of nuclear accidents such as

Chernobyl (estimated $1 \cdot 10^{16}$ Bq ^{90}Sr [24]) and Fukushima Daiichi (estimated $1.4 \cdot 10^{14}$ Bq ^{90}Sr [13]). The Chernobyl contamination of ^{90}Sr is twice the magnitude of the releases as in Fukushima Daiichi due to the different occurrences of the accidents: The Chernobyl accident occurred during operation followed by a nuclear driven explosion and week-long graphite fires, allowing less volatile radionuclides as strontium and plutonium to be released in far distances to the location of accident. The Fukushima Daiichi accident, in contrast, happened because of the failing of reactor cooling after emergency shutdown of the nuclear reactor. Hereby, mostly volatile radionuclides as noble gases, ^{131}I and ^{134,137}Cs were released during hydrogen explosions, venting and the rupture of the primary containment of Unit 2. Less volatile radionuclides were released with contaminated water into the Pacific Ocean [13]. Any natural ^{90}Sr levels as result of spontaneous fission of ^{238}U in the environment cannot be detected with current methods and can be regarded negligible for dose calculations.

The isotope **^{85}Sr** is the only strontium isotope with significant γ emission with an easily usable half-life of 64.8 d. ^{85}Sr decays via electron capture ε and a γ emission at 514 keV with a probability of 96 %. Concerning the properties of ^{85}Sr, the radionuclide is often used as a radiotracer for the determination of the only beta emitting ^{89}Sr and ^{90}Sr. For this purpose, ^{85}Sr can be produced by neutron capture of enriched stable ^{84}Sr [20].

The fission product **^{89}Sr** has a half-life of 50.5 d with a beta endpoint energy of 1500 keV. ^{89}Sr does a beta decays to the stable ^{89}Y. Due to its short half-life, ^{89}Sr is important to consider directly after fallout of nuclear weapon tests and nuclear accidents and has direct contributions to the effective dose. At about 1.5 a after the time of contamination, the only considerably Sr isotope left is ^{90}Sr [5, 20].

1.3.3.2. Radiocesium

One of the commonly produced radioactive products in nuclear fission are isotopes of cesium. Cesium is an alkali metal and is thus very volatile, which enables a high distribution in case of accident. The **^{137}Cs** isotope is a direct fission product with a half-life of 30.07 a and with a fission yield of 6.22 % (^{235}U). Through atmospheric nuclear weapon fallout in the 1950-60s ^{137}Cs is globally distributed with constantly decreasing activity due to the nuclear weapon ban treaty. Local increase of activity can be assigned to location like nuclear accidents and reprocessing plants. ^{137}Cs has one significant γ-emission at 661.7 keV (emission probability: 85.1 %). By contrast the ^{134}Cs isotope is not a direct fission product from nuclear fission, as the 134 isobar ends beforehand on the stable ^{134}Xe. ^{134}Cs can only be produced by neutron activation of the stable fission product ^{133}Cs (neutron capture cross section $\sigma(^{134}Cs)$ = 27.3 barn). Hence, irradiation time for the neutron capture is necessary, which can only be found in reactors and not in weapon tests. Thus, ^{134}Cs is an indicator for nuclear reactor produced radionuclides and can be used to date and locate a younger NPP accident. As the ^{134}Cs has a relatively short half-life (2.07 a), the ^{134}Cs/^{137}Cs ratio can be used to date the contamination directly to one

accident. The $^{134}Cs/^{137}Cs$ ratio at the time of accident in Fukushima Daiichi NPP is estimated to be 1 [1].

Cesium is, as result of chemical similarity to potassium, biological relevant and actively incorporated by the organism. Thus, it is potentially harmful for the organism and one of the main factors for external and internal effective dose over several years after the incident.

1.3.3.3. Radiosilver

Seldom determined radionuclides are radiosilver, respectively **^{108m}Ag** and **^{110m}Ag**. Silver is presumably bio accumulative and therefore as well of interest for dose calculations. Silver is similar volatile as cesium, which enables a similar distribution in case of an accident. The radiosilver isotopes ^{108m}Ag and ^{110m}Ag are not direct fission products, they are produced by neutron activation of silver containing materials or neutron activation of fission products like stable ^{107}Ag or ^{109}Ag . Natural occurring silver has an isotope abundance of ^{107}Ag:^{109}Ag of 52: 48%. Varying fission yields of the stable silver isotopes can lead to different abundances, which might allow to draw conclusions about the origin of activated silver products [25].

1.4. Food safety and monitoring

Food is consumed by humans to provide for nutrition needed to keep body functions alive. Food originates from varies of plants or animals and hold many essential nutrients. These essential nutrients are carbohydrates, fats, proteins, vitamins and minerals. The type and amount of nutrition varies highly with each type of food. In contrast to the organic nutrients, minerals are inorganic material, which the organism needs to take up actively through ingestion as it cannot be produced by the organism itself. Major minerals for mammals are sodium, potassium, calcium, magnesium and phosphorus, which are recommended to uptake in high daily doses. The body needs in far less amounts essential trace elements as iron, zinc, copper, manganese, iodine and selenium.

One of the major essential minerals is calcium. It is recommended to uptake 1000 mg/d for an adult. Calcium is important for bone and teeth structure (99 %), and furthermore intracellular calcium is important for the physiology of the cell in various functions [21].

For the calculation of the effective dose, resulting from the ingestion of contaminated food, the food consumption of the local people is of importance. The annual food consumption pyramid of Japanese people (Figure 7) is adapted from [26]. The Japanese diet contains mainly cereals, in form of rice, with an average of 69 kg/person/a, served with vegetables (39 kg/person/a). Due to Japan being an island, the food consumption highly consists of fish and seafood (14 kg/person/a), whereas in reference to international consumption of meat and animal products, the Japanese portion is rather low (9 kg/person/a).

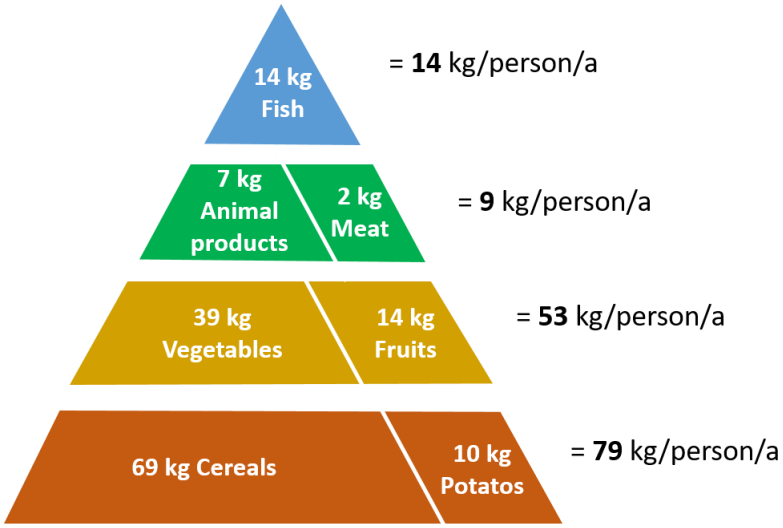

Figure 7: Annual food consumption of Japanese people.

Constant food monitoring after the Fukushima Daiichi NPP accident is of high importance and the Japanese Ministry of Health, Labour and Welfare installed a website with ongoing reports about food contamination analysis:

http://www.mhlw.go.jp/english/topics/2011eq/index_food_radioactive.html.

In the foreground mainly analysis of radiocesium in represented foods of several prefectures are done. Furthermore, every rice bag produced or manufactured in the prefecture Fukushima is controlled.

For the control of radioactive substances in food the Ministry of Health, Labour and Welfare proposed following steps [27]:

1. Establishment of legal limits for radioactive food (Table 4): from the 17th March 2011- 30th March 2012 indicator values from Nuclear Safety Commission were valid and were then substituted by the current legal limits on the 1st of April 2012.
2. Implementation of regular inspection of 100,000 – 400,000 samples of food.
3. Recall and dispose of contaminated food
4. Restriction of the distribution of specific regional foods proposed by the Nuclear Emergency Response Headquarters. Specific prefectures and municipalities, which exceed the legal limits on regular basis, are therefore given a restriction on the distribution of food and need to meet specific requirements for the lifting of the restriction.
5. The legal limits of radionuclides in food were calculated on the assumption, that 50 % of marketed food is contaminated with regards to constantly meeting Japan's food self-sufficiency. The limits take the contribution of radiostrontium,

plutonium, etc. with specific percentages of radiocesium into account. The new limits take age into consideration. For this reason infant food needs to follow stricter regulations. The new legal limits were calculated to not exceed an effective dose from ingestion above 1 mSv/a [5].

Table 4: Japanese established limits of radionuclides in food [27].

Category	**Provisional limits of radioactive cesium in [Bq/kg] from 17th March 2011 until 30th March 2012**	**Limits of radioactive cesium in [Bq/kg] as of 1st April 2012**
Drinking water	200	10
Milk	200	50
General foods	500	100
Infant foods	-	50

The Ministry of Health, Labour and Welfare estimated the effective committed dose resulting from consumption of ^{134}Cs and ^{137}Cs for foods produced in the prefecture Fukushima (samples preferably locally grown) to 19 µSv/a (Sep. 2011) and 3.8 µSv/a (Sep 2012) [27].

2. Materials and methods

2.1. Strontium extraction chromatography

For selective strontium extraction commercially available Sr resin from company eichrom© are used. The strontium selective part is the crown ether 4,4'(5')-di-*t*-butylcyclohexano-18-crown-6 (Figure 8), which has an inner diameter of the crown fitting perfectly to the ionic radius of an strontium cation coordinated by two nitrate anions. 1 % of the crown ether is diluted in 1-octanol and the resulting organic solution embedded on an inert chromatographic stationary phase. The particle size of the chromatographic stationary phase was 50 -100 µm [28].

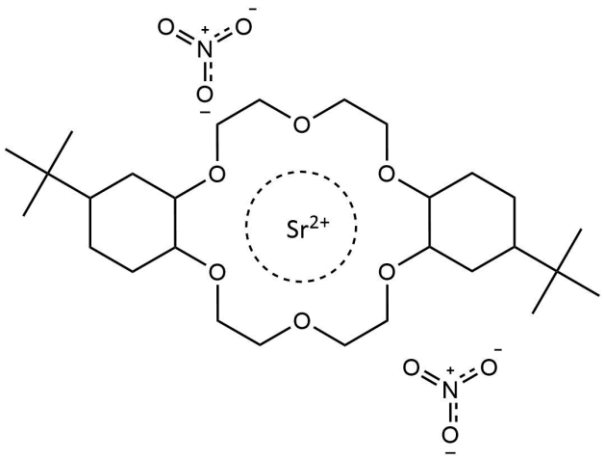

Figure 8: Molecular structure of strontium binding 4,4'(5')-di-*t*-butylcyclohexano-18-crown-6. The Sr binds at high pH values with two coordinated nitrate anions and is released at lesser pH values.

The strontium ion is loaded on the resin with 8 M nitric acid (highest equilibrium constant *k* of 90) and diluted with 0.025 M nitric acid (*k* less than 1). For this reason, an easy separation of strontium from calcium is possible because of calcium's low affinity towards the stationary phase. The barium retention is relatively high on the Sr resin, but has maximal affinity at 3 M nitric acid, in which case a resin loading with 8 M results in washing the Ba off the column. Also tetravalent actinides have significant retention on the Sr column. Through adding of oxalic acid as a competitive complexing agent, the tetravalent actinides are washed from the column. Moreover, complexing agents are also necessary for removing lead, which shows an even higher affinity towards the Sr resin as strontium itself. Interferences from sodium or calcium with concentration less than 0.5 M are not significant, but a calcium mass above 320 mg shows an influence on the chemical yield. Moreover, higher concentration of 0.1 M of potassium show a similar decrease on the chemical yield. In this case previous oxalate precipitation are recommended. The maximal capacity of one Sr resin is 21 mg for a 2 mL column, it is recommended to work at 10-20 % of the maximum capacity. Furthermore, the used particle size has influence on the elution band. A smaller particle size distribution results in narrower elution band but slower flow rates [28, 29].

2.2. Liquid scintillation counting (LSC)

The analysis of the beta emitting ^{90}Sr and daughter nuclide ^{90}Y in environmental samples is performed with liquid scintillation counting (LSC). The used LSC spectrometer is a Hidex 300 SL automatic liquid scintillation counter from Hidex Oy.

The basic principle of LSC is the detection of ionizing radiation in a mixture of the liquid sample with a scintillation cocktail. The mixture of the liquids permits a better efficiency due to higher interaction possibilities than with a solid scintillator. The scintillation cocktail transforms the emitted ionizing radiation into photons in the visible region, which then can be detected by a photomultiplier (PMT). LSC allows the determination of α and β particles.

An LSC instrument consists of an auto sampler for vials (5 -20 mL), a measuring cell with a passive and an active guard system and several PMTs. One vial at each time is put into the measuring cell. The measuring cell is cooled to keep a constant temperature during measurement to avoid thermal excitation and therefore background noise. The cell is surrounded by passive guard. The passive guard consists of a thick wall of lead to reduce the interaction of cosmic rays with the scintillation cocktail. As not all cosmic rays can be shielded from the measuring cell also an active shield is installed in commercially available LSC instruments. The active guard holds a basin with a different liquid scintillation material, which is surrounded by two PMTs. Any count detected inside the measuring cell and the active guard is considered to be from passing cosmic rays and therefore neglected in the analysis. Only emitted photons solely from the measuring cell are defined as a product of radioactive decay. The measuring cell is equipped as well with about two to three PMTs for coincidence measurements. Coincidence measurement allows the registration of almost simultaneously (around 20 ns apart) emitted photons. In the case, that only one photon is registered at one PMT, the chances are high that the photon was produced during different processes (e.g. chemiluminescence) and this event is therefore not included in the analysis [16].

The sample for LSC measurement must be completely separated from matrices to avoid self-absorption and other radiation from radionuclides (e.g. ubiquitous ^{40}K). After the separation the analyte is dissolved in a water phase. The emitted beta particles are also absorbed by the surrounding liquid and cannot reach the detector. Therefore a transformation of the beta energy into photons (e.g. as fluorescence) have the advantages of no or very small absorption in liquids and can be easily detected. The transformation can be done by scintillation cocktails.

Scintillation cocktails consist of solvents and one or more highly aromatic fluorescence active organic molecules. For example the composition of Ultima Gold AB© is 57 – 67% of the solvent diisopropylnaphthaline (DIPN). Furthermore, to allow the mixing of the water sample with the organic compounds solubility enhancer with about 24 – 34% of nonylphenolethoxylate and 2-(2-Butoxyethoxy) ethanol are added to the cocktail. Only some percent of the actual fluorescence active compounds of 2,5-Diephenoloxazol (PPO) and 1-4-bis(2-methylstyryl)benzole (bis-MSB) are found in the cocktail. The emission of beta particles leads to an energy transfer to the solvent molecules and the electrons of the solvent molecule are excited or ionized. Through relaxation processes the excited electrons go back to their electronical ground state. The relaxation can be thermal or through emission of a photon. The

emission of photons occurs up to 10% of all relaxation processes. The emitted photons have energies in the range of X-ray radiation (wavelength around 10-100 pm). These emitted photons can excite the surrounding fluorescence active compounds as PPO, which then again emits photons by relaxation. These photons emit photons of lower energy, close to the weak UV region. For optimizing the detector response of the photomultiplier (PMT), photons with even lower energy are required and for this reason a second fluorescence active compound is excited (e.g. bis-MSB), which emits photons in the visible region. Each emitted beta particle excites several fluorescence molecules at very close time intervals. Therefore, the energy of one beta particle can be described as the sum of the energy of all photons emitted at the same time. Moreover, several different processes need to be taken into consideration for describing the scintillation process correctly. These processes are solvent-solvent transfer, solvent excitation from fluorescence molecule, thermal influence on relaxation and the interaction with foreign particles. All the processes lead to loss in the energy, which is detected [22].

The emitted photons are detected with PMT. Hereby, the photons arrive at a photocathode and produce electrons proportional to the amount of photons. Through voltage gradient, the produced electrons are accelerated towards the secondary electron multiplier (SEM), in which with every passing dynode more electrons are produced. This enables a high multiplying of electrons and a stronger electrical signal. At high temperature dark current can occur, resulting in higher electron releases due to thermal processes. For this reason - to avoid dark current – cooling of the equipment is recommended [30].

In liquid scintillation the effect of quenching has a high influence on the detectable signal. Due to interaction of the produced photons within the sample solution, the counting signal can be increased/decreased or a shift in the detected energy might occur. For this reason, it is important to know the exact composition of the solution. Three different quenching processes are differentiated in respect to their origin: Colour, chemical and physical quenching. Colour quenching emerges when specific atoms or molecules in the solution adsorb the fluorescence emitted photons and for this reason the detectable signal decreases. For example a solution tinted brown (iron cations) adsorbs photons with complementary colours. Furthermore, chemical quenching occurs by electron absorbing from chemical reagents, leading to a decrease in the photon yield. The third quenching process is the physical quenching, in which the fluorescence photons are partially adsorbed again by the solvent and the excited molecule relaxes through thermal processes as vibration, translation and intersystem-crossing without the emission of radiation. Another physical quenching type is the light scattering process at suspended particles. Possible quenching effects – especially with high variation of the analysing matrix – needs to be taken into consideration. Quenching can be corrected with different methods: a calibration with different quenching matrices with an external radiation source (e.g. ^{226}Ra source) or the measurement of a triple to double coincidence ratio (TDCR). The used LSC

Spectrometer Hidex 300 SL I equipped with a TDCR measurement system. Both the double and triple coincidences are measured simultaneously with three triangle coordinated photomultipliers. The ratio of the triple to double coincidence is afterwards calculated. The triple coincidences is far more effected by quenching effects than the double coincidence. Experiments confirmed that for pure beta emitting radionuclides, the TDCR is proportional by 1 to the overall efficiency of the LSC. Therefore the quench level automatically calculated with the TDCR as an absolute method [30].High energy beta emitters (> 1500 keV) can be directly measured with liquid scintillation counting without scintillation cocktails due to the Cerenkov Effect. The Cerenkov Effect produces Cerenkov radiation when charged particles move faster than the phase velocity in a clear dielectric medium. For example Cerenkov radiation can be used for the radionuclides ^{32}P and ^{90}Y.

The LSC measurement is an energy resolved method. This allows a distinction of radionuclides with high differences in their beta endpoint energies. However, each beta spectrum of a radionuclide is a continuous spectrum and therefore limits the resolution due to overlapping spectra. For the analysis of ^{85}Sr and ^{90}Sr with ingrowing daughter nuclide ^{90}Y a three window method is proposed [31]. In Figure 9 a complete spectrum of all three radionuclides is shown with the split individual spectra and background. The three windows are placed at the last channel of the individual spectra. Window 2 can be used for the sole analysis of ^{90}Sr right after the separation of the daughter nuclide, whereas both Window 2 and 3 can be used for the determination of the complete activity of $^{90}Sr/^{90}Y$ after the complete ingrowth of ^{90}Y at 14 days.

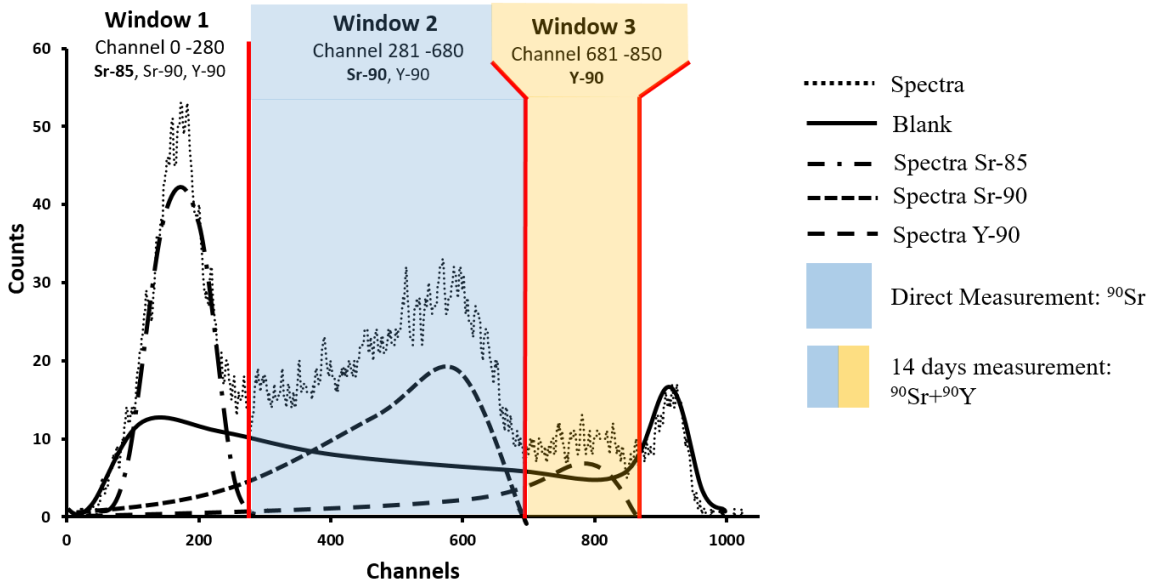

Figure 9: LSC beta spectra of ^{85}Sr, ^{90}Sr and ^{90}Y with characteristic spectra lines for each radionuclide and blank. The three windows for analysis are separated with red lines. The direct analysis for ^{90}Sr is done with window 2, whereas after 14 days the activity determination of the combined activity of ^{90}Sr and ingrown ^{90}Y is done with window 2 and 3. Window 1 can be used for yield determination with ^{85}Sr.

2.3. Gamma spectroscopy with semiconductors

One of the main methods for surveillance of environmental radioactivity is the gamma spectroscopy with semiconductor materials. The most popular semiconductor material is high-purity germanium (HPGe) because of its high energy resolution with a combining good efficiency and low sample preparation time.

A HPGe gamma spectroscope has four main instruments: a germanium crystal with a Dewar basin with liquid nitrogen, a lead and cooper shield, electronics and a data processor [16].

The semiconducting germanium crystal consists of n-doped (electron excess) and p-doped (hole excess) germanium, which are joined together. The holes and electrons migrate at the PN junctions towards the side, which contains less of the charge. The migration continues until a macroscopic equilibrium is reached and the space charge region is build. The PN semiconductor is operated in reverse bias mode by applying positive voltage towards the n-doped side and negative voltage to the p-doped side. This results in an increase of the depletion layer, which is the active detector volume. In the case a γ- quant deposits its energy through ionisation in the depletion layer, electron-hole pairs are produced. The amount of produced electron-hole pairs are proportional to the deposited energy. The free charges are accelerated towards the electrodes with the applied electrical field and produce an electrical signal. This signal is amplified with a preamplifier and then pulse height amplifier. Thereafter, the analogue signal is transformed into a digital signal for data processing [16].

Gamma rays are high energy electromagnetic radiation with discrete energy lines, resulting from discrete nuclei energy levels. Many radionuclides emit γ-rays in the range from 20 keV up to 10 MeV. Gamma rays have different interaction mechanism with the detector volume: Photoelectric effect, Compton Effect and pair production. The dominant effect depends on the energy of the gamma ray. At energies < 100 keV the photoelectric effect, between 100 and 5000 keV the Compton Effect and above 5 MeV the pair production is dominant.

The photoelectric effect is the preferable effect for gamma spectroscopy because the gamma ray deposits its whole energy inside detector volume. The gamma photon interacts with a bonded electron of the semiconductor crystal and produces a photoelectron with almost the complete energy of the photon (except the binding energy of the electron). Through following cascade reactions of the photoelectron with valence electrons free charges proportional to the energy of the gamma photon are produced and lead to nuclide specific full-energy peaks. The Compton Effect is the elastic scattering of the photon with outer shell electrons of the semiconductor atoms. The energy transfer from the photon is thereby strongly dependent on the scattering angle θ and this produces a Compton continuum in the background spectrum. The maximal transferred energy is at backscattering (θ = 180 °) and visible as the Compton edge in a spectrum. The third effect is the pair production. This effect can occur at energies higher

than 1022 keV (double rest mass of the electron) and is dominant at above 5 MeV. The pair production describes the interaction of a high-energy photon with the coulomb field of a nucleus, which results in an electron-positron pair. The sum of the kinetic energy of the produced electron and positron corresponds to the difference of the energy of the γ photon and the double rest mass of the electron. In the same manner, an interaction of the produced electron and positron leads to annihilation under the emission of two photons with the characteristic energy of 511 keV. Annihilation peaks can be observed in the gamma spectra at E_γ - 511 keV (single escape peak) and E_γ - 1022 keV (double escape peak) [16].

2.4. Chemicals and materials

Chemicals:

- Calcium carbonate ($CaCO_3$) p.a. from Merck®
- Acetic acid (CH_3COOH, ω = 100%) p.a. from VWR chemicals®
- Yttrium chloride hexahydrate ($YCl_3 \cdot 6\ H_2O$) from Sigma Aldrich®
- Strontium chloride from Sigma Aldrich®
- Hydrochloric acid (HCl, ω = 37 %) p.a. from VWR chemicals®
- Nitric acid (HNO_3, ω = 69 %) ACS from Merck®
- Oxalic acid dihydrate ($C_2H_2O_4 \cdot 2\ H_2O$) ACS from Merck®
- Methyl red sodium salt from Alfa Aesar®
- Ammonia (NH_3, ω = 25 %) ACS from Merck®
- Di-Ammonium oxalate monohydrate ($(NH_4)_2C_2O_4 \cdot H_2O$) ACS from Merck®
- Ethanol from Merck®
- ^{85}Sr stock solution (9,622 kBq/g at 01.07.2016) from physikalisch-technischen Bundesanstalt Braunschweig und Berlin (PTB)
- Diluted ^{85}Sr solution (965 Bq/ml at 26.08.2016)
- ^{90}Sr stock solution (73.3 Bq/mL)
- Diluted ^{90}Sr solution (0.733 Bq/mL at 23.08.2018)
- Ultima Gold AB™ LSC Cocktail from PerkinElmer Inc. (57-67 % Di-isopropylnaphthaline (DIN), 24-34 % Nonylphenolethoxylate, 2-(2-Butoxyethoxy)ethanol, 2,5-Diphenoloxazol (PPO) and 1-4-Bis(2-methylstyryl)benzol (bis-MSB))
- Sr carrier solution (4.8 mg Sr^{2+} per mL)
- Y carrier (4 mg Y^{3+}per mL)
- 36.6 kBq/g QCY-48 Standard from PTB

Materials:

- Sr Resin (Particle size: 50-100 µm, 50x2 mL) from eichrom®
- Porcelain dish (Ø = 11 cm)

- Quartz crucible
- Multielement-standard
- Petri dish (Ø = 9.5 cm)
- Ashless round filter
- Stainless steel grid

2.5. Instrumentation and software

Instrumentation:

- Hidex 300 SL Automatic liquid scintillation counter (Hidex Oy)
- Muffle furnace from Heraeus thermicon P®
- HPGe Detectors (Appendix E: Certificates)

Software:

- MikroWin 300 SL
- Gamma Acquisition & Analysis

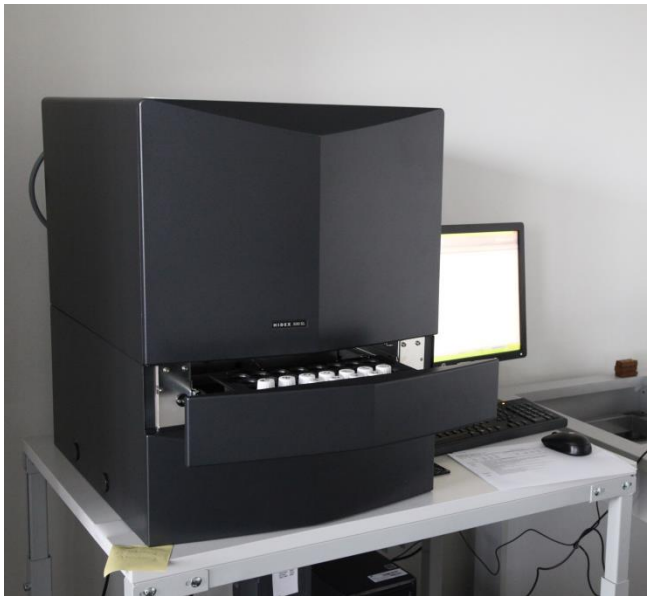

Figure 10: Liquid scintalliation counter (LSC) Hidex 300 SL from Hidex OY with TDCR technology.

2.6. Experiment

2.6.1. Sampling

The sampling was done by Ass.-Prof. Dr. Katsumi Shozugawa from the University of Tokyo, Japan. Altogether 37 samples differing from basic foods (rice, wheat), fish, seafood, vegetables and fruits, mushrooms and luxury foods (tea, coffee) were taken from different prefectures around Japan. The sampling dates ranged from May 2015 to September 2016. The sampling location is presented in Figure 11. Some samples were already manufactured at the time of sampling and the exact location is unknown. Thus, these samples are not presented. The exact information of the 37 samples can be found in the Appendix D: Additional information. Most samples were collected on the east side of Japan towards the Pacific Ocean within a 300 km area from the Fukushima Daiichi nuclear power plant. Furthermore, a reference mushroom sample was taken in Russia (distance of 3600 km to Fukushima Daiichi). Most of the samples were shipped in an already hackled/ground and freeze-dried state.

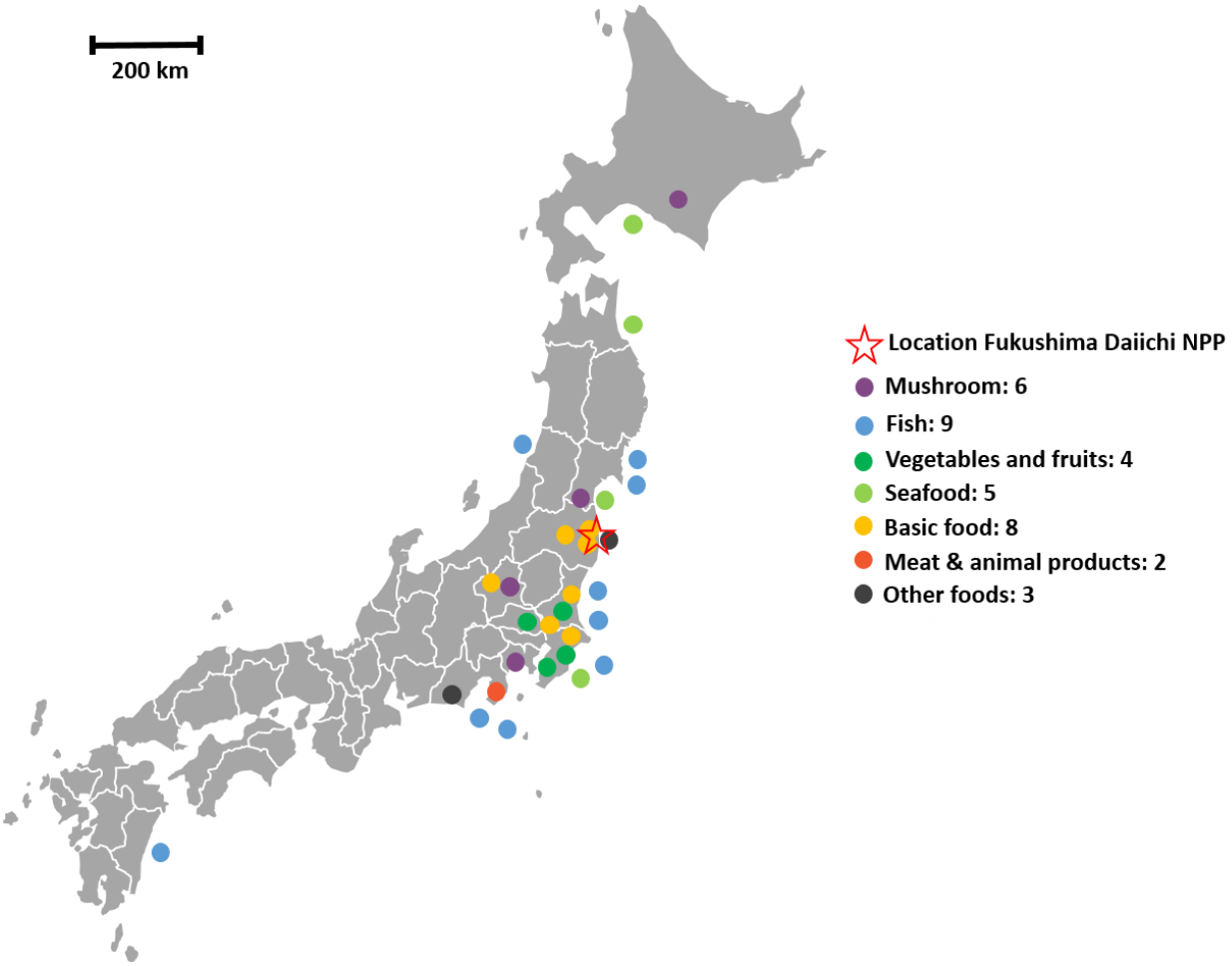

Figure 11: Sampling location of different kinds of food across Japan. Manufactured foods, where the original location is unknown, are not represented in the map.

2.6.2. Gamma spectroscopic measurement of food concentrates

To determine the ^{134}Cs and ^{137}Cs activity of the samples, the samples were filled into petri dishes (Ø = 9.5 cm). Then, the samples were measured at a high-purity germanium (HPGe) detector. Due to varying sample density, the efficiency of ^{134}Cs and ^{137}Cs were determined using a multielement-surface standard. Hereby, the efficiency of ^{134}Cs was calculated using the Jaeckel-Westmeier-equation.

2.6.3. Preparation of food concentrates

All 37 samples were provided by Ass.-Prof. Dr. Katsumi Shozugawa from The University of Tokyo. Previously, the samples were mostly freeze-dried or ashed before shipping to Germany to minimize the sample weight and volume. The sample preparation steps were adapted from Nordmeyer [32]. For every sample the same sample preparation procedure as described below was used. The seawater sample was an exception: The sample preparation started after the 1st incineration step.

The sample (5 - 50 g) was divided into two aliquots and was weighted onto an ashless round filter in a porcelain dish. One aliquot was used for beta analysis. The first 10 prepared samples were spiked with 10 Bq ^{85}Sr. The sample, which was covered with a stainless steel grid, was incinerated in a muffle furnace. The detailed temperature programme is presented in Table 5. If the ash was not yet white-grayish, the sample was ashed a second time.

The cooled ash was rinsed with 50 mL distilled water into a beaker. For a complete oxalate precipitation, approximately 0.2 g calcium carbonate was added to the solution. Afterwards, the solution was acidified using 5 mL conc. hydrochloric acid and 1 mL conc. nitric acid. The solution was heated to its boiling point. Then, after cooling, the solution was filtrated and washed three times with 10 mL hot 10 % solution of hydrochloric acid and three times with 10 mL distilled water.

Subsequently, the strontium was co-precipitated with calcium as an oxalate. In this step, 8 mL saturated oxalic acid solution were added. Following the addition of some drops of methyl red indicator dye solution (colour transition: pH = 4.4 - 6.2), resulting in a pink solution. Then, concentrated 25 % ammonia solution was slowly added until the solution turns yellowish and white sediment was observed. Acetic acid was added until an orange colour became noticeable. After a cooling down phase, the precipitation is finished and the completeness of the precipitation was tested with some drops of saturated ammonium oxalate solution. The precipitate was filtrated and washed with three times 10 mL distilled water, once with 10 mL saturated oxalate solution and once with 10 mL ethanol. The precipitate on the filter was ashed in a muffle furnace with temperature programme 2 (Table 5).

Firstly, a few drops of water were added to the white oxide sediment, following a slow addition of 10 mL 8 mol/L nitric acid solution. The solution was heated to its boiling point and cooled down again. The solution was filtrated and the filter washed three times with 8 mol/L nitric acid solution.

For the extraction of strontium, 2 mL cartridges of Sr-Resin from eichrom© were used. The resin was conditioned with three times 5 mL 8 mol/L nitric acid. Then, the acidified sample was pipetted onto the resin. The sample container was washed three times with 5 ml 8 mol/L nitric acid solution. To avoid contamination with foreign ions, the resin was washed three times with 3 mol/L nitric acid containing 0.25 mol/L oxalic acid. For the elution of strontium the resin is washed three times 5 mL with 0.025 mol/L nitric acid into a flask containing 5 mg Y^{3+} and 5 mg Sr^{2+} carrier. The solution was evaporated to about 1 mL and filled up to 4 mL with distilled water. The sample solution is homogenised with 16 mL Ultima Gold AB© solution in a 20 mL LSC plastic vial for LSC measurement.

Table 5: Temperature programme of the 1st and 2nd incineration step.

	1st Incineration step		2nd Incineration step	
Heating stage	**Temperature**	**Time**	**Temperature**	**Time**
1	20 °C → 250 °C	20 min	20 °C → 250 °C	20 min
2	250 °C	20 min hold	250 °C	20 min hold
3	250 °C → 400 °C	30 min	250 °C → 400 °C	30 min
4	400 °C	30 min hold	400 °C	30 min hold
5	400 °C → 500 °C	20 min	400 °C → 500 °C	20 min
6	500 °C	20 min hold	500 °C	20 min hold
7	500 °C → 620 °C	30 min	500 °C → 900 °C	30 min
8	620 °C	3 h	900 °C	3 h
9	620 °C → 20 °C	10 h	900 °C → 20 °C	10 h

2.6.4. LSC measurement

The samples were measured right after the preparation at the Hidex 300 SL Automatic liquid scintillation counter to avoid the ingrowth of ^{90}Y. A blind sample containing 4 mL prepared milk powder and 16 mL LSC Ultima Gold AB was measured as control. The cool down phase was 4 h and every standard was measured four times for each 2.5 hours and every sample four times 5 hours for repeatability studies. The LSC spectra were evaluated in three windows: channel 0 – 250 (^{85}Sr), 251-650 (^{90}Sr) and 651-820 (^{90}Y). After about 14 days with almost reaching the secular equilibrium of ^{90}Sr and ^{90}Y, the samples were measured again.

2.6.5. Time dependent elution of Strontium

For testing the time dependence on the elution of strontium of the Sr Resin (eichrom®), the resin was loaded with ^{85}Sr (700 – 350 Bq) and left for different time intervals on the resin, varying between 8 weeks and direct elution. The elution followed the same steps like the elution of the samples: three times 5 mL washing with 3 M nitric acid with 0.25 M oxalic acid, and elution with three times 5 mL 0.025 M nitric acid. The eluate was filled up to 20 mL in a petri dish. For each time interval, three identical samples were measured for repeatability studies. The ^{85}Sr activity of all samples and control, containing ^{85}Sr standard solution, was measured with an HPGe detector on the same day with each sample having the same activity of 363 Bq and with identical geometries prior and after the ion chromatography.

3. Results and discussion

3.1. Optimizing of sample preparation steps

3.1.1. Chemical yield determination of sample preparation

The preparation steps of the strontium extraction were optimized by controlling the chemical yield of ^{85}Sr with gamma spectroscopy for each preparation step. For this experiment, 5 blanks (milk powder) were spiked with 200 Bq of ^{85}Sr and prepared after the instruction of chapter 2.6.3. The yield was determined after each step with a standard of ^{85}Sr in the same geometry and is listed in Table 6. The uncertainties result from the relative standard deviation of the five analysed samples.

Table 6: Chemical yield of the preparation steps.

Preparation step	Yield ^{85}Sr [%]
1. Incineration 1	93.2 ± 2.8
2. Precipitation	92.7 ± 6.5
2. Incineration 2	96.9 ± 2.4
Extraction load fraction	6.8 ± 4.6
Extraction wash fraction	3.6 ± 1.1
Extraction Sr resin	6.1 ± 0.5
Extraction Sr fraction	65 ± 15

The steps of incineration and precipitation are implemented in the sample preparation to eliminate the disturbing organic matrices and alkali metals such potassium and sodium. The chemical yield of the gamma emitting ^{85}Sr of these preparation steps was above 90%. For this reason, the incineration and precipitation has proven to be a good way to eliminate disturbing elements without unacceptable losses of analyte in a complex matrix such as foods. The main loss of the strontium analyte takes place in the strontium extraction with the Sr specific resin. The Sr resin manufacture's data (Appendix E: Certificates) ensures a chemical yield of strontium above 85%. Losses occur in the load fraction, wash fraction and the remaining of analyte on the resin. With several preparation steps ahead of the strontium extraction the overall chemical yield of ^{85}Sr in the described sample preparation of foods is 65 ± 15%. The worst determined chemical yield was 60.2%, which is used as the yield for not ^{85}Sr spiked samples. Although the use of a ^{85}Sr tracer offers a straightforward and reliable method to determine the yield of the Sr extraction, it also has several disadvantages in LSC measurements of ^{90}Sr (cf. Chapter 3.2.1.). Therefore, the ^{85}Sr radiotracer was no longer used after the measurement of 10 samples. An alternative yield determination may be possible with adding stable strontium to the sample. In this case, the strontium concentration is measured in the blank and known amounts of tracer are added. Afterwards, the stable strontium is measured in the prepared solution. The measurement of stable strontium can be done with ICP-OES (^{90}Sr amount negligible) or ICP-MS. It is important not to exceed the limit capacity of strontium of 8 mg Sr^{2+} with the stable tracer on the resin.

3.1.2. Stability of Sr resins in long-term usage

The stability of Sr resins was tested on the condition of long-term exposure to high acidity (loading solution 8 M nitric acid). For this reason, ^{85}Sr was loaded on the resin in 8 M nitric acid and afterwards the closed resin was stored for 3 days up to 2 months. For each time interval three replicates were done. Then, the ^{85}Sr was eluted after the storage time and the chemical yield was determined with gamma spectroscopy with a reference ^{85}Sr solution with the same geometry. The chemical yield after different time intervals from load until elution is presented in Figure 12. No significant influence with the time for the elution of strontium became apparent. This allows the usage of the strontium specific resin for pre accumulation of strontium over a long time interval. Furthermore, the Sr resin can be loaded with strontium, and after 14 days fractions of ingrown ^{90}Y and of ^{90}Sr can be eluted. The chemical yield of ^{85}Sr in the strontium fraction is 86 – 89%, which correlates with the manufacturer's data.

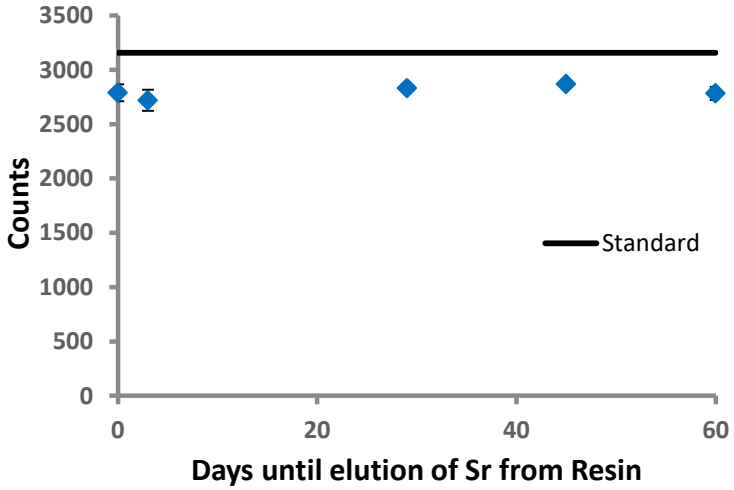

Figure 12: Chemical yield of ^{85}Sr in dependence of the time of elution from Sr resin.

3.2. Evaluation of Three Window Method

3.2.1. Setting of the Windows and calibration curves

The evaluation for the ^{90}Sr activity is performed with the Three Window Method for LSC measurements [31]. The counts are registered at an LSC spectra with 1024 channels. These 1024 channels are assigned to specific energy regions with a logarithmic scale. For this reason, beta emissions with lower energy have a higher resolution. Beta emissions with medium high energy (e.g. β^-_{end}(^{90}Sr) = 546 keV) are mostly located in medium channels. Whereby high energy beta emissions as β^-_{end}(^{90}Y = 2240 keV) are mostly detected in higher channels, with some effects in all lower channels (cf. Figure 9). Due to various quenching effects and instrument parameters, the following definition of regions for the strontium quantification is only valid for

the described method. For varying matrices and instruments, the channel region might need to be adjusted. The three windows for the radionuclide analysis are set at:

1. Window 1: Channel 0 – 280 (**^{85}Sr**, ^{90}Sr, ^{90}Y): The main component in this region is the gamma emitting tracer nuclide ^{85}Sr. Furthermore, it has significant counts from continuous spectra of ^{90}Sr. The counts resulting from the spectra of ^{90}Y are negligible.
2. Window 2: Channel 281 - 680 (^{85}Sr, **^{90}Sr**, ^{90}Y): The counts in this defined region mostly result from the radionuclide ^{90}Sr. Direct after the separation of ^{90}Sr, this region does not have counts from the continuous spectra of ^{90}Y. However, as the measurement time of each samples is 24 hours, significant ingrowth of ^{90}Y can be noticed and the ingrowth needs to be corrected in this region. After almost reaching the secular equilibrium after 14 days, the count rate in window 2 and 3 can be used for the overall determination of the total activity of ^{90}Sr and ^{90}Y. Moreover, the ^{85}Sr isotope has a significant Compton background in this window 2 [22]. Therefore, the usage of ^{85}Sr as a chemical yield tracer was only done in the 10 first measurements and at the following 27 measurements the tracer was abstained. For the chemical yield the worst-case in model experiments (60.2%) was used.
3. Window 3: Channel 681 – 820 (**^{90}Y**): Window 3 detects only the radionuclide ^{90}Y and does not suffer any interferences by other radionuclides in the prepared strontium extract. Window 3 can be used to determine the ingrowth of the daughter radionuclide ^{90}Y and at reaching almost the secular equilibrium after 14 days for activity determination in combination with Window 2 for a lower detection limit at the double of the initial activity of ^{90}Sr.

The linear calibration curve for Window 2 (Channel 280 - 680) direct after separation from the daughter nuclide ^{90}Y is presented in Figure 13 a). The calibration is used for the determination of ^{90}Sr directly after the matrix separation. For the determination of the total activity of ^{90}Sr/^{90}Y after an ingrowth time of 14 days, the calibration curve for ^{90}Sr/^{90}Y of Windows 2 and 3 (Channel 280 – 820) is used.

To test the linearity of the calibration curve, the Mandel's fitting test (Eq. 3.1) is performed [33], with the number of calibration standards *N* = 6 and the variance of the linear function $s_{e,1}^2$ and the quadratic function $s_{e,1}^2$. In both calibration curve cases the F_{test} value was below the $F_{\alpha,1,\text{N-3}}$ with 99 % statistically certainty, therefore the hypothesis of linear calibration is accepted.

$$F_{\text{test}} = \frac{(N-2)s_{e,1}^2 - (N-3)s_{e,2}^2}{s_{e,2}^2} \tag{3.1}$$

For testing of potential outliers in the calibration curve a simple F-Test (Eq. 3.2) with and without the potential outliers were done. All tested calibration points were $F_{\text{test}} < F_{\alpha,1,N_2\text{-}2}$, no significant outliers could be found.

$$F_{\text{test}} = \frac{(N_1 - 2)s_{e,1}^2 - (N_2 - 2)s_{e,2}^2}{s_{e,2}^2} \tag{3.2}$$

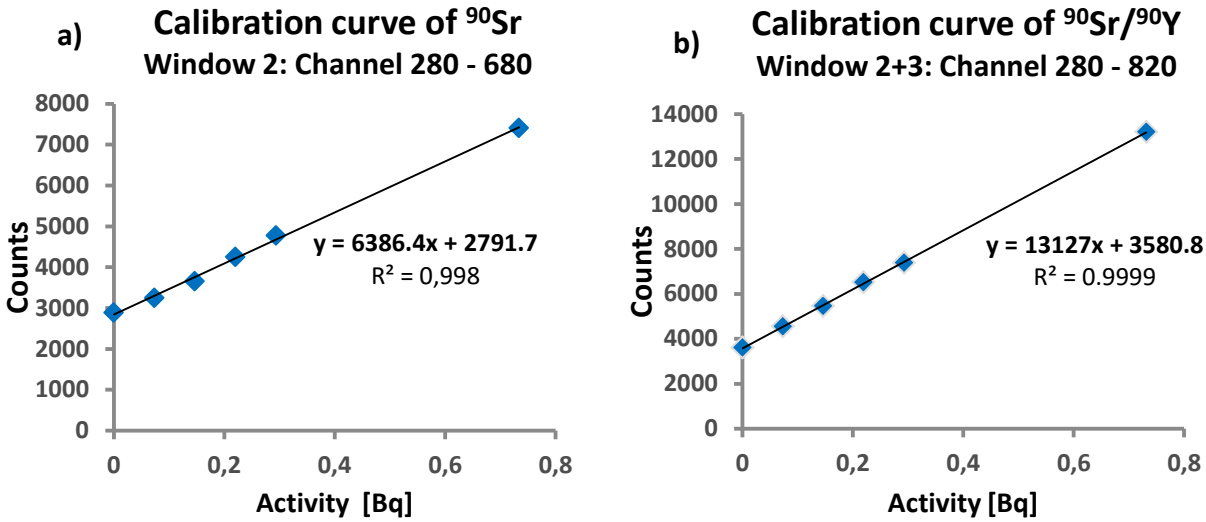

Figure 13: LSC measurement calibration curves for a) Window 2 (Channel 281 – 680) for the determination of ^{90}Sr in freshly separated samples and b) Window 2 + 3 (Channel 281 - 820) for the activity determination of ^{90}Sr and ingrown daughter nuclide ^{90}Y.

3.2.2. Determination of characteristic limits

The characteristic limits of the calibration curves were determined using the DIN ISO 32645 [34]. The DIN Norm differentiates between the blank value method and the calibration curve method for the determination of the limit of detection (LOD) and limit of quantification (LOQ). In this thesis, the calibration curve method was used for both calibration curves.

The residual standard deviation of a calibration function s_e can be calculated with Eq. 3.3 with the number of calibration standards *N*, y_i values of the measurement, $\hat{y}_i$ values of the regressive linear calibration.

$$s_e = \sqrt{\frac{\sum(y_i - \hat{y}_i)^2}{N - 2}} \tag{3.3}$$

The critical y-value y_{crit} is calculated with Eq. 3.4 and depends on the y-intercept y, the *t*-distribution $t_{\text{f},\alpha}$ with the degree of freedoms f and probability $(1 - \alpha) = 95\%$, the residual standard deviation s_{e}, number of calibration standards N, number of repeat measurements M, the mean of the x values $\bar{x}$, the standard deviation of the gradient s_a.

$$y_{\text{crit}} = a + t_{\text{f},\alpha} \cdot s_{\text{e}} \cdot \sqrt{\frac{1}{N} + \frac{1}{M} + \frac{\bar{x}^2}{s_a}} \tag{3.4}$$

Afterwards, the limit of detection can be calculated with linear calibration function (Eq. 3.5) with the critical y-value and the slope *b*.

$$x_{\mathrm{LOD}} = \frac{y_{\mathrm{crit}} - a}{b} \tag{3.5}$$

Table 7: Parameters of the calculation of the limit of detection and quantification for the calibration function for ^{90}Sr and for ^{90}Sr/^{90}Y.

	Calibration curve ^{90}Sr Window 2 (Channel 280 - 680)	**Calibration curve ^{90}Sr/^{90}Y** Window 2 + 3 (Channel 280 - 820)
a	6250.6 Bq^{-1}	13587Bq^{-1}
b	2840.6	3699
$\overline{x}$	0.2446 Bq	0.2440 Bq
s_e	82.76	91.23
N	6	6
s_a	141.7	156.6
x_{LOD}	0.0397 Bq	0.0201 Bq
x_{LOQ}	0.1192 Bq	0.0604 Bq

For these values statistically errors needs to be taken into consideration: Type I error and type II error. The type I error (false positive) rejects the zero hypothesis but it is true. The type II error (false negative) accepts the hypothesis even though it is false.

The limit of detection (LOD) allows a qualitative statement, if the analyte is inside the sample or not. The type I error is 5 % and the type II error 50 % for the LOD value. The relative result uncertainty is 100 %. The limit of quantification (LOQ) allows a quantitative determination of the analyte amount inside the sample and is the lowest working region. The relative result uncertainty is below 50 %. For analyte values above the quantification limit, confidence intervals (CI) can be used for specification of the analyte uncertainty. The LOD value is 40 mBq/vial (^{90}Sr) and 20 mBq/vial (^{90}Sr+^{90}Y). Therefore, the trace analysis of ^{90}Sr with ingrown ^{90}Y allows a detection of about 4 fg of ^{90}Sr per vial.

3.3. Determination of ^{90}Sr in food concentrates

The analyte activity is determined using the DIN 38402-51 [35]. The analyte activity can be calculated using the calibration function (Eq. 3.6) for measured counts in Window 2 and respectively Window 2+3.

$$x = \frac{y - a}{b} \tag{3.6}$$

The confidence interval (CI) of the measured value can be calculated with Eq. 3.7 with the mean of the *x* values $\bar{x}$.

$$u(x_i) = \frac{s_e \cdot t_{0.95,5}}{b} \cdot \sqrt{\frac{1}{M} + \frac{1}{N} + \frac{(y_i - \bar{y})^2}{b^2 \cdot \sum(x_i - \bar{x})}} \tag{3.7}$$

3.3.1. Test sample ^{90}Sr determination

For testing of the LSC, three window method two milk powder blank samples were spiked with ^{90}Sr: Test 1 (0.073 Bq ^{90}Sr) and Test 2 (0.142 Bq ^{90}Sr). For samples containing ^{85}Sr, corrections for ^{85}Sr Compton background in the region of Window 2 were made. Following steps for the correction was made for the first 10 measured samples:

1. The counts of ^{90}Sr in Window 1 were less than 100 at activities below or even 0.146 Bq ^{90}Sr, this presents less than 2.5 % of the counts registered in Window 1 for 10 Bq of ^{85}Sr and was neglected at the determination of ^{85}Sr activity. However, the 2.5 % was added as uncertainty of the ^{85}Sr activity calculation.
2. The activity of ^{85}Sr in the samples was calculated at Window 1 with a calibration function (Appendix D: Additional information).
3. The Compton background resulting from ^{85}Sr in Window 2 was calculated from the determined ^{85}Sr activity in Window 1 with the calibration curve of Window 2. The calculated counts from the Compton background are subtracted from the counts in Window 2.
4. The corrected counts in Window 2 can be used for the determination of ^{90}Sr activity.

The Table 8 presents the calculated and chemical yield-corrected activities of the spiked test solution for the direct determination of ^{90}Sr after extraction and for the sum activity of ^{90}Sr+^{90}Y. The chemical yield for the samples without radiotracer is estimated with the worst determined yield of 60.3%. Tests 1 and 2 show good comparability of the determination from the activity of ^{90}Sr with the calculated sum activity of ^{90}Sr/^{90}Y within their uncertainties. The calculation of the corrected activity with the chemical yield of strontium has values above the actual activity as intended.

Table 8: ^{90}Sr spiked test solutions with the calculated and chemical yield corrected activity.

Tests	Spiked activity	Calculated activity [mBq]	Chemical yield [%]	Corrected activity [mBq]
Test 1: ^{90}Sr	73 mBq ^{90}Sr	44 ± 25	60.2	73 ± 40
Test 1: ^{90}Sr + ^{90}Y	73 mBq ^{90}Sr	47 ± 7	60.2	78 ± 12
Test 2: ^{90}Sr	146 mBq ^{90}Sr	100 ± 24	60.2	166 ± 40
Test 2: ^{90}Sr + ^{90}Y	146 mBq ^{90}Sr	96 ± 7.5	60.2	160 ± 13

3.3.2. Real sample ^{90}Sr determination

The real food concentrates samples from Japan were analysed using the described Three-Window Method and the analytical results are reported in Table 9. The first 10 samples have added radiotracer ^{85}Sr (marked with *), whereas the following 27 samples were measured without the radiotracer. The analysed sample material mass per vial varied strongly from 3 to 150 g.

All samples originating from Japan (sampling dates: March 2015 – September 2016) had no detectable contamination of ^{90}Sr. However, ^{90}Sr could be detected in a mushroom sample from Russia, the ^{90}Sr activity in the vial was above the detection limit of 20 mBq/Vial ^{90}Sr/^{90}Y but below the quantification limit of 60 mBq/Vial ^{90}Sr/^{90}Y. The specific activity of ^{90}Sr/^{90}Y in the mushroom sample lies between these limits with 4.1 Bq/kg$_{mush}$ < x < 12.3 Bq/kg$_{mush}$ with an uncertainty of 100 %.

Investigation on ^{90}Sr in several food samples with sampling dates between May 2011 and November 2013 were performed Nabeshi et al. [5]. Some of these investigated food samples contained ^{90}Sr in detectable quantities (fresh weight samples: 0.029 ± 0.008 Bq/kg (Shiitake mushroom) – 0.87 ± 0.08 Bq/kg (Horsetail)). Dried samples as mulberry leaf tea have ^{90}Sr activities with up to 5.5 Bq/kg. However, the amounts did not significantly vary from measured ^{90}Sr activities in food samples before the Fukushima Daiichi NPP accident. Furthermore, no correlation between the radiocesium and the radiostrontium content could be found.

Neither the investigations of ^{90}Sr in foodstuffs in this master thesis nor from Nabeshi et al. [5] have found significant ^{90}Sr contaminated foods from the fallout of the Fukushima Daiichi NPP accident. The low ^{90}Sr contents in some foods from Nabeshi et. al. probably originated from the global fallout. It is highly possible, that the in this master thesis investigated food samples contained ^{90}Sr in low levels as well, that could not be detected due to low mass of the analysed samples.

Table 9: The analyzed 37 food concentrated from Japan ordered after the food category and their distances to the Fukushima Daiichi NPP. Furthermore, the mass of the raw portion and the determined $^{90}Sr/^{90}Y$ activity is given. *marked foods have added radiotracer ^{85}Sr and the Compton background was corrected for the analysis.

Food category	Food	Distance from Fukushima NPP [km]	Analysed raw portion [g]	$^{90}Sr/^{90}Y$ activity [Bq/kg_{raw}]
Mushroom	Fukushima mushroom	35	54.76	< LOD
	Miyagi mushroom	95.2	95.76	< LOD
	Gumma mushroom	189	76.15	< LOD
	Kanagawa mushroom	306	7.01	< LOD
	Hokkaido mushroom	491.1	10.32	< LOD
	Russian mushroom	3600	4.86	4.1 < x < 12.3
Fish	Miyagi flatfish	95.2	50.81	< LOD
	*Yamagata taro	111.7	152.02	< LOD
	*Ibaraki sardines	127	54.55	< LOD
	Pond smelt	160.4	16.71	< LOD
	*Chiba dorado	217	78.24	< LOD
	Shizuoka tuna	374.4	7.90	< LOD
	Miyazaki whitebait	1071	40.24	< LOD
	Miyagi bonito	-	36.71	< LOD
	Boiled fish paste	-	32.50	< LOD
Vegetable and fruit	Ibaraki blueberry	181	70.71	< LOD
	Blueberry paste	214	63.69	< LOD
	*Chiba carrot	217	48.77	< LOD
	*Chiba peanuts	217	16.12	< LOD
Seafood	Miyagi oyster	95	84.10	< LOD
	Chiba abalone	218	41.69	< LOD
	Aomori squid	346.9	79.51	< LOD
	Hokkaido abalone	629	64.60	< LOD
	Baked seaweed	695	5.46	< LOD
Basic food	*Namiem rice	11.1	24.70	< LOD
	*Naraha rice	15.9	23.68	< LOD
	Tamura brown rice	40.4	10.83	< LOD
	Ibaraki sweet potato	127	38.37	< LOD
	Chiba brown rice	201	12.17	< LOD
	*Chiba brown rice	217	55.30	< LOD
	*Gumma rice	230.8	42.70	< LOD
	Iwate wheat	254	10.26	< LOD
Animal product	Wild boar jerkey	335	8.95	< LOD
	Skimmed milk	-	8.42	< LOD
Other food	Sea water	0.6	91.56	< LOD
	*Kagekawa tea	401	14.97	< LOD
	Instant coffee	-	3.31	< LOD

3.4. Gamma spectroscopic investigation of ^{134}Cs and ^{137}Cs in food concentrates

The energy and efficiency calibration of the HPGe detectors were performed with a round surface multi nuclide QCY-48 standard with following characteristics (Table 10). The γ-emission of the radionuclide ^{203}Hg was not used, as it was almost completely decayed at the time of measurement. The certificate from Eckert&Ziegler is attached in the Appendix E: Certificates.

Table 10: The calibration standard QCY-48 from Eckert & Ziegler Isotope Products is from 1st May 2016. The standard solution was soluted with a factor of 0.0255. * ^{203}Hg was almost completely decayed at time of usage of the standard. For this reason, it was not considered for energy, efficiency or activity calculations.

Nuclide	Gamma ray energy [keV]	Half-life [d]	Branching ratio [%]	Specific Activity [Bq/g]	Total Uncertainty [%]
^{241}Am	60	157,742 ± 241	36.0	27.54	3.1
^{109}Cd	88	462.6 ± 0.7	3.63	392.8	2.5
^{57}Co	122	271.79 ± 0.09	85.6	12.29	2.3
^{139}Ce	166	137.64 ± 0.023	79.9	17.39	2.3
^{203}Hg*	279	46.595 ± 0.013	81.5	54.57	2.3
^{113}Sn	392	115.09 ± 0.04	64.9	69.87	2.3
^{85}Sr	514	64.849 ± 0.004	98.4	84.66	2.3
^{137}Cs	662	11,012 ± 58	85.1	59.16	2.3
^{88}Y	898	106.63 ± 0.025	94.0	136.17	2.3
	1836		99.4		2.3
^{60}Co	1173	1,924 ± 0.4	99.86	70.64	2.3
	1333		99.98		2.3
Total activity				4,794	

3.4.1. Energy calibration

The QCY-48 standard has 10 radionuclides with 12 significant γ-lines, which covers the working energy regions (60 – 1836 keV) of the HPGe detectors. The location of the gamma peaks with their specific energy and the full-width half maximum (FWHM) can be assigned to the channels *C* with the quadratic polynoms (Eq. 3.8 and 3.9) with the operating software Ginnie2k®.

$$E(C) = A_0 + A_1 C + A_2 C^2 \quad (3.8)$$

$$FWHM(C) = B_0 + B_1 C + B_2 C^2 \quad (3.9)$$

3.4.2. Efficiency calibration

The uncertainties of a function with uncorrelated variables (Eq. 3.10) are calculated with error propagation (Eq. 3.11) after the Guide to the Expression of Uncertainty in Measurement GUM.

$$f(x_1, x_2, \ldots, x_n) \tag{3.10}$$

$$u_f = \sqrt{\left(\frac{\partial f}{\partial x_1} \cdot u_{x_1}\right)^2 + \left(\frac{\partial f}{\partial x_2} \cdot u_{x_2}\right)^2 + \cdots + \left(\frac{\partial f}{\partial x_n} \cdot u_{x_n}\right)^2} \tag{3.11}$$

After complete energy calibration of the gamma system, an efficiency calibration for the activity calculation is performed. The efficiency of a gamma detector (Eq. 3.12) describes the ratio of the net count rate $r_n\ (E)$ and the actual gamma emission rate $r_{emit}(E)$. The uncertainty of the efficiency can be described with error propagation with Eq. 3.13.

$$\epsilon(E) = \frac{r_n\ (E)}{r_{emit}(E)} \tag{3.12}$$

$$u(\epsilon) = \epsilon(E) \cdot \sqrt{u^2(r_{net}) + u^2(r_{emit})} \tag{3.13}$$

The efficiency is highly dependent on the energy of the emitted gamma quant. The higher the energy, the less likely the energy of the gamma quant is fully deposited within the detector crystal volume (photo effect) and the efficiency decreases. At low energies the possibility of adsorption of the gamma quant in air, sample container or in the entry window (material dependence) increases, resulting as well in a lower efficiency. A good interpolation of the efficiency curve is done with the Jaeckel-Westmeier equation (Eq. 3.14). Through fitting the parameters c_i of the Jaeckel-Westmeier equation, radionuclide activities with different energies from the multi nuclide standard can determined (e.g. ^{134}Cs: 604.7 keV, 798.5 keV; ^{40}K: 1460 keV).

$$\epsilon(E) = e^{\frac{2}{\pi}\left(c_1 + c_2 \cdot \ln(x) + c_3 \cdot \ln(x)^2\right) \cdot \arctan\left(e^{c_4 + c_5 \cdot \ln(x) + c_6 \cdot \ln(x)^3}\right) - 25} \tag{3.14}$$

Gamma rays are exponentially weakened in matter. The extent of the weakening depends highly on the energy of the gamma ray and the kind of weakening matter. A sample of a significant height has significant absorption effects. For this reason, the efficiency is highly dependent on the geometry of the sample. For the used Petri dish geometry, the efficiency calculation was performed with the foil method described by Solle [18]. The foil method uses a round surface area standard (filter paper: Ø = 10 cm) to measure the efficiency on the top (Eq. 3.15) and the bottom (Eq. 3.16) of the Petri dish containing the sample. As the circumstances require the net count rate *r* needs to be corrected by the net count rate resulting from the same nuclide in the sample r_{Sample} (e.g. ^{137}Cs: 661.7 keV).

$$\epsilon_{top} = \frac{r_{top} - r_{Sample}}{r_{emit}} \tag{3.15}$$

$$\epsilon_{\text{bot}} = \frac{r_{\text{bot}} - r_{\text{Sample}}}{r_{\text{emit}}} \tag{3.16}$$

The efficiency of the sample can be calculated as the logarithmic mean of the efficiency on the top and bottom of the Petri dish with Eq. 3.17. The uncertainty of the efficiency is calculated with Eq. 3.18.

$$\epsilon_i = \frac{\epsilon_{\text{bot}} - \epsilon_{\text{top}}}{\ln(\epsilon_{\text{bot}}) - \ln(\epsilon_{\text{top}})} = \frac{\Delta\epsilon_i}{\Delta \ln(\epsilon_i)} \tag{3.17}$$

$$u(\epsilon_i) = \sqrt{\frac{(\Delta\epsilon_i - \epsilon_{\text{bot}} \cdot \Delta \ln(\epsilon_i))^2 \cdot u_{\text{rel}}^2(\epsilon_{\text{bot}}) + \left(\Delta\epsilon_i - \epsilon_{\text{top}} \cdot \Delta \ln(\epsilon_i)\right)^2 \cdot u_{\text{rel}}^2(\epsilon_{\text{top}})}{\Delta\ln(\epsilon_i)^4}} \tag{3.18}$$

3.4.3. Activity determination of undisturbed discrete gamma emissions

The determination of the gamma activity and the characteristic limits were performed with the DIN 11929 [36]. In the first step, the net count rate of the area of the radionuclide r_{net} is calculated as the difference of the initial area count rate r_{ini} and the zero effect count rate r_0 (Eq. 3.19). The used software Genie2K© automatically reports the net count rate and uncertainty (Eq. 3.20).

$$r_{\text{net}} = r_{\text{ini}} - r_0 = \frac{n_{\text{ini}}}{t_{\text{ini}}} - \frac{n_0}{t_0} \tag{3.19}$$

$$u(r_{\text{net}}) = \sqrt{\frac{u^2(n_{\text{ini}})}{t_{\text{ini}}^2} + \frac{u^2(n_0)}{t_0^2}} \tag{3.20}$$

Afterwards, the specific activity *a* can be calculated with the summations corrections factor k_s, the sample mass m, the efficiency ϵ and the emission probability p_γ (Eq.3.21). The summations correction factors (k_s(^{137}Cs) = 1, k_s(^{134}Cs) = 1.11; k_s(^{40}K) = 1) and the emission probability are taken from literature. The uncertainty of the specific activity is calculated with error propagation with Eq. 3.22.

$$a = \frac{k_s}{m \cdot \epsilon \cdot p_\gamma} \cdot r_{\text{net}} = w \cdot r_{\text{net}} \tag{3.21}$$

$$u(a) = \sqrt{w^2 \cdot u^2(r_{\text{net}}) + r_{\text{net}}^2 \cdot u_{\text{rel}}{}^2(w)} \tag{3.22}$$

with $u_{\text{rel}}^2(w) = u_{\text{rel}}^2(k_s) + u_{\text{rel}}^2(m) + u_{\text{rel}}^2(\epsilon) + u_{\text{rel}}^2(p_\gamma)$. (3.23)

Each of the 37 food concentrate samples were investigated for ^{134}Cs, ^{137}Cs and ^{40}K activity with gamma spectroscopy. The calculated specific activities of the radionuclides are presented in Table 11. The measurement time for each sample were at least one day.

Table 11: Determined specific activities of ^{134}Cs, ^{137}Cs and ^{40}K in various foods, ordered after food category and in dependence on distance to the Fukushima NPP. In red: radiocesium contamination above the legal limit of 100 Bq/kg.

Food category	Food	Distance from Fukushima NPP [km]	Weighed raw portion [g]	^{134}Cs activity [Bq/kg_{raw}]	^{137}Cs activity [Bq/kg_{raw}]	^{40}K activity [Bq/kg_{raw}]
Mush-room	Fukushima mushroom	35	143.93	0.45 ± 0.04	3.46 ± 0.09	102 ± 2
	Miyagi mushroom	95.2	299.61	4.6 ± 0.2	16.5 ± 0.3	43.5 ± 2.6
	Gumma mushroom	189	235.10	4.3 ± 0.2	19.4 ± 0.4	123 ± 4
	Kanagawa mushroom	306	18.56	31.7 ± 1.4	127 ± 2	1216 ± 26
	Hokkaido mushroom	491.1	14.26	< LOD	< LOD	1260 ± 58
	Russian mushroom	3600	15.15	< LOD	53 ± 2	1926 ± 4
Fish	Miyagi flatfish	95.2	159.03	< LOD	< LOD	161 ± 6
	Yamagata taro	111.7	356.01	< LOD	< LOD	166 ± 4
	Ibaraki sardines	127	124.26	< LOD	< LOD	478 ± 10
	Pond smelt	160.4	53.94	< LOD	12.3 ± 1.3	229 ± 12
	Chiba dorado	217	172.97	< LOD	< LOD	186 ± 6
	Shizuoka tuna	374.4	25.26	< LOD	< LOD	682 ± 18
	Miyazaki whitebait	1071	150.28	< LOD	< LOD	99 ± 2
	Miyagi bonito	-	105.10	< LOD	< LOD	218 ± 8
	Boiled fish paste	-	88.24	< LOD	< LOD	37 ±2
Vegetable and fruit	Ibaraki blueberry	181	220.79	< LOD	< LOD	72 ± 2
	Blueberry paste	214	154.86	< LOD	1.2 ± 0.1	30.1 ± 1.1
	Chiba carrot	217	98.53	< LOD	< LOD	207 ± 8
	Chiba peanuts	217	29.33	< LOD	< LOD	569 ± 16
Sea-food	Miyagi oyster	95	252.79	< LOD	< LOD	36.7 ± 0.7
	Chiba abalone	218	126.44	< LOD	< LOD	72 + 1
	Aomori squid	346.9	215.24	< LOD	< LOD	128 ± 5
	Hokkaido abalone	629	169.42	< LOD	< LOD	94 ± 2
	Baked seaweed	695	14.82	< LOD	< LOD	1096 ± 26
Basic food	Namiem rice	11.1	45.94	< LOD	< LOD	243 ± 15
	Naraha rice	15.9	46.58	< LOD	< LOD	268 ± 16
	Tamura brown rice	40.4	31.82	< LOD	< LOD	87 ± 4
	Ibaraki sweet potato	127	122.20	< LOD	< LOD	225 ± 4
	Chiba brown rice	201	39.78	< LOD	2.4 ± 0.2	163 ± 2
	Chiba brown rice	217	122.79	< LOD	< LOD	84 ± 8
	Gumma rice	230.8	117.16	< LOD	< LOD	111 ± 7
	Iwate wheat	254	31.91	< LOD	< LOD	58 ± 4
Animal product	Wild boar jerkey	335	27.03	5.9 ± 0.5	36.4 ± 1.4	242 ± 20
	Skimmed milk	-	26.44	< LOD	< LOD	909 ± 36
Other food	Sea water	0.6	308.93	0.71 ± 0.06	0.69 ± 0.09	37.2 ± 1.1
	Kagekawa tea	401	29.08	< LOD	< LOD	768 ± 28
	Instant coffee	-	10.79	< LOD	< LOD	2268 ± 97

Most samples did not exceed the limit of detection. However, characteristic foods, which are known for the accumulation of radiocesium, as mushrooms, seafood and wild animals show significant radiocesium contamination. All analysed food sample have radiocesium contaminations below the current legal limit of 100 Bq/kg $^{134+137}$Cs with the exception of a mushroom sample from Kanagawa (306 km from Fukushima Daiichi NPP), which shows a $^{134+137}$Cs contamination (160 Bq/kg) above the current legal limits. The mushroom sample from Kanagawa is not allowed to be distributed by the Japanese law. Some specific food samples with significant radiocesium contamination are presented on a map of Japan (Figure 14).

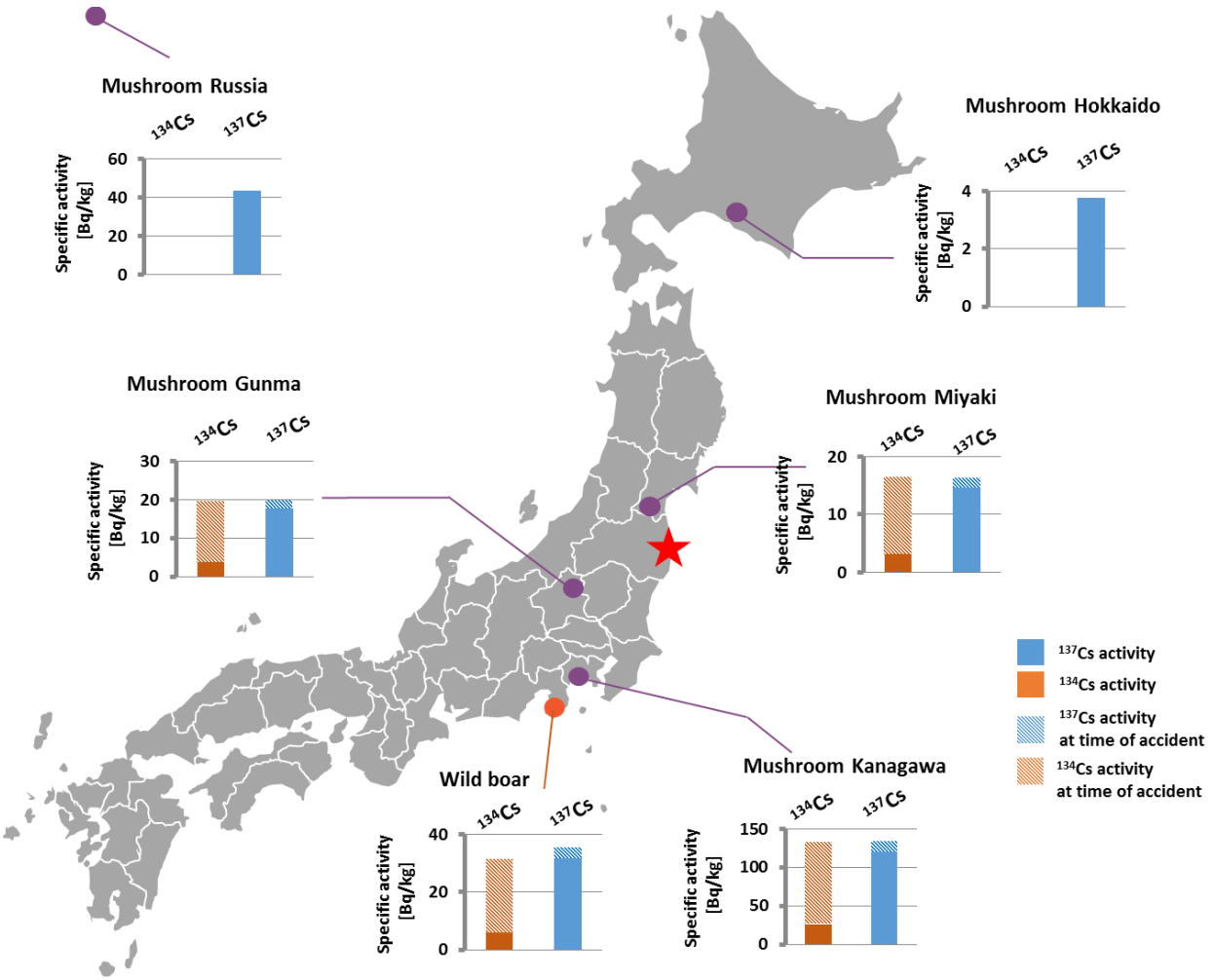

Figure 14: Location of specific analysed food samples in January 2016 with significant radiocesium contamination, mainly mushrooms. In a 300 km radius around the location of the Fukushima NPP accident, the relatively short-lived ^{134}Cs ($t_{1/2}$ = 2.065 a) can be determined. The ratio ^{134}Cs/^{137}Cs calculated back to the time of the Fukushima NPP accident is about 1 and therefore characteristic for the accident. Samples from further away have values of ^{134}Cs below the detection limit; this allows the attribution of the ^{137}Cs to atmospheric nuclear weapon fallout.

The mushroom samples from Russia and Hokkaido only have minor ^{137}Cs contamination, which indicates its origin from previous sources, most likely nuclear weapon fallout. Food samples around a 350 km radius around the Fukushima NPP show ^{134}Cs contamination, which is produced by neutron activation after significant irradiation times in a nuclear reactor. The emission of relatively short-lived ^{134}Cs ($t_{1/2}$= 2.065 a) indicates a lately release in a nuclear accident. For this reason, the ratio of $^{134}Cs/^{137}Cs$ activities can date the release of the radiocesium. Figure 14 shows the ^{134}Cs and ^{137}Cs specific activity corrected to the time of accident on the 11th March 2011. The ratio at the time of accident is around 1, which enables an attribution of the radiocesium releases to the Fukushima Daiichi NPP accident.

The mushroom sample from Russia has detectable ^{90}Sr contamination (4.1 Bq/kg$_{mush}$ < x < 12.3 Bq/kg$_{mush}$) and ^{137}Cs contamination (53 ± 2 Bq/kg). However, as no ^{134}Cs contamination is present, the ^{90}Sr contamination most probably does not originate from a recent NPP accident. The contamination possibly originates from ubiquitous nuclear weapons fallout in the northern hemisphere.

The determined radiocesium activities correlates well with the values from the radiocesium determination of the food samples done by Dr. Katsumi Shozugawa, University of Tokyo (cf. Appendix D: Additional information). However, the detection limits of the gamma measurement from Japan are lower due to higher sample volumes and lower background in Japan. This enables a detection of radiocesium in more samples.

Cesium is a potassium analogue and cesium uptake correlates with the mineral content of the analysed food. Potassium has a natural abundance of 0.012% of the primordial radionuclide ^{40}K. For this reason, the main component of the ingestion radiation exposure results from the ^{40}K content of the essential nutrients. Therefore, the ^{40}K activity is a good indicator for the mineral content in food. If the food is exposed to radiocesium, it is actively incorporated by the plant or animal as potassium analogue. For this reason a high actively incorporation of potassium results in higher radiocesium contamination (e.g. mushrooms). Table 11 shows that foods with radiocesium contamination mostly have high contents of ^{40}K as well.

3.4.4. Determination of radiosilver in food

Furthermore, the gamma analysis has shown the presence of radiosilver isotopes in seafood samples with specific activities up to 57 mBq/kg ^{110m}Ag (Miyagi oyster). The radiosilver isotopes ^{108m}Ag and ^{110m}Ag cannot be produced directly by fission, which obstructs an origin as of nuclear weapon fallout. The radiosilver isotopes are primarily produced by neutron activation of the stable silver isotopes ^{107}Ag and ^{109}Ag at long irradiation times only found in nuclear power plants. The stable silver isotopes in a NPP can be found in silver containing material or as fission products. Silver is similarly volatile as cesium and has a possible widespread contamination after the Fukushima Daiichi NPP accident.

Table 12: Radiosilver specific activity in seafood samples, measurement results by Dr. Katsumi Shozugawa (Appendix D: Additional information).

	^{108m}Ag ($t_{1/2}$ = 438 a) [mBq/kg$_{raw}$]	^{110m}Ag ($t_{1/2}$ = 250 d) [mBq/kg$_{raw}$]
Miyagi oyster	8.9 ± 1.6	56.8 ± 1.5
Hokkaido abalone	32.3 ± 5.1	-
Chiba abalone	32.7 ± 7.7	-

3.5. Estimation of ingestion dose

The estimation of the annual ingestion dose, resulting from the consumption of the analysed food samples were calculated with the Eq. 1.16. The food consumption habits of Japanese people were taken from [26], the radionuclide specific dose coefficients are from [37]. The specific activity of the food categories equals the highest contaminated food sample in the category. In the case, that no radionuclide could be detected in the food category, the detection limit regarding the lowest analysed mass of sample was taken. The calculated ingestion dose (Table 13) is valid for the worst possible case of ingestion of contaminated food. The resulting ingestion dose is only estimation. For this reason, no uncertainties due to high varying personal food consumption habit are given.

The worst-case annual effective dose through ingestion of the food is for every analysed fission product below 100 µSv/a and the ^{90}Sr/^{137}Cs ratio around 10 %. The yearly ingestion dose of the primordial radionuclide ^{40}K exceeds the effective dose of the anthropogenic radionuclides considerably.

However, in respect to ^{90}Sr, the biological accumulation as calcium analogue in bone and teeth structure is considerably high and the biological half-life $t_{1/2,\mathrm{bio}}$ of strontium around 20 years. For the estimation of the effective dose in the following 10 years, the effective half-life of the radionuclide $t_{1/2,\mathrm{eff}}$ needs to be considered (Eq. 3.24) with the physical half-life $t_{1/2,\mathrm{phy}}$ and the biological half-life $t_{1/2,\mathrm{bio}}$.

$$t_{1/2,\mathrm{eff}} = \frac{t_{1/2,\mathrm{phy}} \cdot t_{1/2,\mathrm{bio}}}{(t_{1/2,\mathrm{phy}} + t_{1/2,\mathrm{bio}})} \tag{3.24}$$

Table 13: Estimation of the worst-case annual ingestion dose, resulting from consumption of the analysed 37 samples. The calculation used the highest found radionuclide contamination in the samples and it was extrapolated to the food consumption of Japanese adults from [26]. *including mushrooms. **in respect to the detection limit with the smallest analysed mass of sample in the food category.

Radio-nuclide	Food category	Food con-sumption [kg/a]	Dose coefficient [Sv/Bq] [37]	Specific activity [Bq/kg_{raw}]	Worst-case annual ingestion dose [µSv/a]
^{90}Sr	Cereals	79	$3.07 \cdot 10^{-8}$	**1.95	4.3
	*Vegetables	53	$3.07 \cdot 10^{-8}$	**2.85	4.2
	Fish	14	$3.07 \cdot 10^{-8}$	**2.53	1.0
	Animal products	9	$3.07 \cdot 10^{-8}$	**2.38	0.6
					10.1
^{134}Cs	Cereals	79	$1.9 \cdot 10^{-8}$	**1.23	1.8
	*Vegetables	53	$1.9 \cdot 10^{-8}$	24.6 ± 1.4	24.8
	Fish	14	$1.9 \cdot 10^{-8}$	**1.23	0.3
	Animal products	9	$1.9 \cdot 10^{-8}$	5.4 ± 0.5	0.9
					28
^{137}Cs	Cereals	79	$1.3 \cdot 10^{-8}$	2.3 ± 0.2	2.4
	*Vegetables	53	$1.3 \cdot 10^{-8}$	125 ± 2	86.1
	Fish	14	$1.3 \cdot 10^{-8}$	12.1 ± 1.3	2.2
	Animal products	9	$1.3 \cdot 10^{-8}$	36.2 ± 1.4	4.2
					94
^{40}K	Cereals	79	$6.2 \cdot 10^{-9}$	163 ± 2	80
	*Vegetables	53	$6.2 \cdot 10^{-9}$	1926 ± 4	632
	Fish	14	$6.2 \cdot 10^{-9}$	229 ± 12	20
	Animal products	9	$6.2 \cdot 10^{-9}$	242 ± 20	14
					746

The calculated effective half-lives of the analysed radionuclides are presented in Table 14. Radiocesium has due to its similarity to potassium a relative short biological half-life and therefore a short effective half-life. This results in a relatively small cumulated effective ingestion dose in 10 years after the consumption. However, as an effect of the long biological half-life of strontium, the cumulated effective ingestion dose after 10 years is continuously and significantly increasing over the years. This underlines the importance of constant surveillance and ultra-trace analysis of ^{90}Sr.

Table 14: The effective half-life of radionuclides ^{90}Sr, ^{134}Cs, ^{137}Cs and ^{40}K inside the organism and the calculated effective dose in the following 10 years after one-time annual ingestion.

	Physical half-life	Biological half-life	Effective half-life	Cumulated effective ingestion dose after 10 a [µSv/a]
^{90}Sr	28.9 a	20 a [22]	11.8 a	93
^{134}Cs	2.065 a	130 d [38]	88 d	32
^{137}Cs	30.08 a	130 d [38]	99 d	113
^{40}K	$1.25 \cdot 10^9$ a	16 d [39]	16 d	746

4. Conclusion

The sample preparation for ^{90}Sr beta analysis with LSC was optimized with the analysis of the losses of the analyte in various preparation steps. For this purpose, gamma-emitting ^{85}Sr was used for chemical yield determination. The incineration and precipitation steps for eliminating disturbing organic matrices and alkali metals cause only marginal losses of the analyte. Therefore, these steps are meaningful and recommendable for the ^{90}Sr analysis in various food matrices. The highest loss of the analyte was found in the strontium extraction step with the Sr resin, which only guarantees a chemical yield above 85%. The worst chemical yield of all preparation steps with 60.2% was used as the yield for sample measurements without radiotracer.

The analysis of ^{90}Sr was done in a three windows approach on LSC spectra. The first window served the determination of the radiotracer ^{85}Sr. The radiotracer was only used for the 10 first samples, as ^{85}Sr has shown significant Compton electron background in higher channels, which results in worse detection limits and higher uncertainties due to correction demand. The following 27 samples were therefore measured without the radiotracer and the worst case chemical yield – determined with ^{85}Sr spiked blank samples – at 60.2 % was assumed. Quenching effects in the LSC spectra can be neglected as the standards and the samples all have the same matrices due to various preparation steps ahead of the LSC measurement and due to automatic quench correction in the TDCR mode of the HIDEX 300 SL liquid scintillation counter.

Low detection limit values could be determined with the calibration curve method of DIN 32645. For the pure beta emitting ^{90}Sr, right after the strontium extraction, 40 mBq/vial was determined and allows fast analysis in case of emergency situations within 3 days after sampling. A detection limit of 20 mBq/vial for the whole activity of ^{90}Sr and complete ingrown ^{90}Y after 14 days after strontium extraction could be determined, this detection limit corresponds to a detection of 4 fg ^{90}Sr per vial. The detection limit for the specific activity in food is highly dependent on the sample amount. No detectable contamination of ^{90}Sr in food concentrates from Japan with sampling dates of 2015 – 2016 could be found, the amounts were below the detection limit of 20 mBq/vial. One mushroom (Inonotus obliquus) sample from Russia showed increased values of ^{90}Sr above the level of detection (> 15 mBq/vial; 4.1 $Bq/kg_{mush} < x < 12.3\ Bq/\ kg_{mush}$) but below level of quantification. Since no ^{134}Cs contamination was present in the sample, the origin of the anthropogenic radionuclide is probably due to atmospheric nuclear weapons fallout. The presented results are in good agreement with the literature: Previously investigated food samples from the years 2011-2013 from Nabeshi et al. could also not find any ^{90}Sr contamination from the Fukushima Daiichi NPP accident fallout.

The determined ^{134}Cs and ^{137}Cs activities from the investigated food samples show good correlation with the values determined by our collaborating partner Dr. Katsumi Shozugawa from the University of Tokyo. Samples from a radius around 350 km show a $^{134}Cs/^{137}Cs$ activity ratio, which calculated back to the time of the accident is approximately 1, and therefore an indicator of contaminations of the fallout from the Fukushima Daiichi NPP accident. One mushroom sample from the prefecture Kanagawa has a total radiocesium contamination of 160 Bq/kg, which is above the current regulatory limit of 100 Bq/kg. This food must not be distributed in Japan.

Furthermore, radiosilver was found in seafood samples of oyster and abalones. The origin of the radiosilver isotopes ^{108m}Ag and ^{110m}Ag are is neutron activation of stable silver isotopes; that can occur either in materials exposed to the reactor's neutron flux or from the stable fission products ^{107}Ag and ^{109}Ag. Due to similar volatility of silver to cesium, a high distribution during the accident might have been possible and further studies are needed for the investigation of this finding.

Moreover, the annual effective dose from ingestion of the investigated food samples was calculated for the worst-case contamination found. The food consumption for the calculation was adapted to the eating habits of the Japanese people in four food categories (cereals, vegetables, fish and animal products). The effective dose for ^{90}Sr was calculated on behalf of the limit of detection and the smallest analysed sample amount in the food category. In the worst-case an annual effective dose of 11 µSv/a was received. The effective dose from the radionuclides ^{134}Cs and ^{137}Cs was calculated with the highest specific activity of each food category. The worst-case effective dose from ^{134}Cs is 28 µSv/a and ^{137}Cs is 94 µSv/a, respectively. The highest impact on effective ingestion has the natural occurring primordial radionuclide ^{40}K with a calculated maximal dose of 746 µSv/a. Radiostrontium has relatively long biological half-life (in contrast to cesium and potassium). For this reason, the cumulated effective dose from the ^{90}Sr ingestion dose is considerably higher than for radiocesium. Therefore, a constant surveillance is always of high importance in food safety policy.

5. References

[1] G. Steinhauser, A. Brandl, and T. E. Johnson, “Comparison of the Chernobyl and Fukushima nuclear accidents: A review of the environmental impacts,” (eng), *The Science of the total environment*, vol. 470-471, pp. 800–817, 2014.

[2] Ministry of Health, Labour and Welfare, *Level of Radioactive Contaminants in Foods Tested in Respective Prefectures.* [Online] Available: http://www.mhlw.go.jp/english/topics/2011eq/index_food_radioactive.html. Accessed on: Mar. 13 2017.

[3] S. Merz, G. Steinhauser, and N. Hamada, “Anthropogenic radionuclides in Japanese food: Environmental and legal implications,” (eng), *Environmental science & technology*, vol. 47, no. 3, pp. 1248–1256, 2013.

[4] S. Merz, K. Shozugawa, and G. Steinhauser, “Analysis of Japanese radionuclide monitoring data of food before and after the Fukushima nuclear accident,” (eng), *Environmental science & technology*, vol. 49, no. 5, pp. 2875–2885, 2015.

[5] H. Nabeshi *et al.,* “Surveillance of Strontium-90 in Foods after the Fukushima Daiichi Nuclear Power Plant Accident,” *Food Hygiene and Safety Science*, vol. 56, no. 4, pp. 133–143, 2015.

[6] G. Steinhauser, V. Schauer, and K. Shozugawa, “Concentration of Strontium-90 in Selected Hot Spots in Japan,” *PLOS ONE*, vol. 8, no. 3, e57760, 2013.

[7] U. Büttner *et al., Fukushima Daiichi 11. März 2011: Unfallablauf, radiologische Folgen*. Köln: GRS, 2012.

[8] M. B. Raap, “The Impact of Mixed Oxide Fuel Use on Accident Consequences at Fukushima Daiichi: American Nuclear Society Technical Brief -March 2011,” 2011.

[9] “Fukushima Daiichi: ANS Committee Report: Appendix G,” *American Nuclear Society*, 2012.

[10] Argonne National Laboratory, “Spent Fuel,” http://www.ne.anl.gov/pdfs/nuclear/spent_fuel_nutt.pdf, Apr. 2011.

[11] M. Ragheb, “Decay heat generation in fission reactors,” *University of Illinois*, 2011.

[12] TEPCO, “The Development of and Lessons from the Fukushima Daiichi Nuclear Accident,” *Tokyo electric power company*, 2013.

[13] ENSI, “Auswirkung Fukushima 11032011: Radiologische Auswirkungen aus den kerntechnischen Unfällen in Fukushima vom 11.03.2011,” *Eidgenössisches Nuklearsicherheitsinspektorat ENSI*, 2011.

[14] UNSCEAR, *Exposures and effects of the Chernobyl accident: Annex J*. New York, 2000.

[15] H.-G. Vogt and H. Schultz, *Grundzüge des praktischen Strahlenschutzes*: Carl Hanser Verlag München Wien, 2011.

[16] J.-V. Kratz and K. H. Lieser, *Nuclear and Radiochemistry: Fundamentals and Applications,* 3rd ed. Weinheim, Germany: Wiley-VCH GmbH & Co, 2013.

[17] R. Michel, “Radionuklide: Gesundheitsschäden durch strahlende Lebensmittel,” 2010.
[18] A. Solle, “Gammaspektrometrie an Bodenproben von als Ackerland genutzten Auenflächen der Vereinigten Mulde,” 2010.
[19] “Joint Evaluated Fission and Fusion File, Incident-neutron data,” http://www-nds.iaea.org/exfor/endf00.htm, 2006.
[20] National Nuclear Data Center, *Chart of Nuclides.* [Online] Available: http://www.nndc.bnl.gov/chart/chartNuc.jsp.
[21] A. Holleman and E. Wiberg, *Lehrbuch der Anorganischen Chemie,* 81st ed. Berlin: Walter de Gruyter, 1976.
[22] A. Mewis, “Strontium-90 in der Umwelt: Migrationsverhalten im Boden, Transfer in die Nahrungskette und Strahlenexposition in der nördlichen Ukraine: Dissertation,” vol. 2004.
[23] Y. Takagai, M. Furukawa, Y. Kameo, and K. Suzuki, “Sequential inductively coupled plasma quadrupole mass-spectrometric quantification of radioactive strontium-90 incorporating cascade separation steps for radioactive contamination rapid survey,” *Anal. Methods*, no. 6, pp. 355–362, 2014.
[24] UNSCEAR, *Sources and effects of ionizing radiation: Annex D*.
[25] H. Lepage *et al.,* “Environmental mobility of (110m)Ag: Lessons learnt from Fukushima accident (Japan) and potential use for tracking the dispersion of contamination within coastal catchments,” (eng), *Journal of environmental radioactivity*, vol. 130, pp. 44–55, 2014.
[26] N. Maruchi, S. Aoki, K. Tsuda, Y. Tanaka, and H. Toyokawa, “Relation of food consumption to cancer mortality in Japan, with special reference to international figures,” (eng), *Gan*, vol. 68, no. 1, pp. 1–13, 1977.
[27] Department of Environmental Health and Food Safety, “Radioactive materials in foods: - current situation and protective measures -,” *Ministry of Health, Labour and Welfare*, pp. 1–21, http://www.mhlw.go.jp/english/topics/2011eq/dl/food-130926_1.pdf, 2012.
[28] A. Alvarez, N. Navarro, and S. Salvador, “New method for90Sr determination in liquid samples,” *Journal of Radioanalytical and Nuclear Chemistry, Articles*, vol. 191, no. 2, pp. 315–322, 1995.
[29] E. P. Horwitz, M. L. Dietz, and R. Chiarizia, “The application of novel extraction chromatographic materials to the characterization of radioactive waste solutions,” *Journal of Radioanalytical and Nuclear Chemistry, Articles*, vol. 161, no. 2, pp. 575–583, 1992.
[30] Hidex, “Hidex 300 SL Automatic liquid scintillation counter: Owner's handbook,” 2014.
[31] J. Eikenberg, H. Beer, M. Rüthi, I. Zumsteg, and A. Vetter, “Precise determination of 89Sr and 90Sr/90Y in various matrices: the LSC 3-window approach,” *LSC 2005, Advances in Liquid Scintillation Spectrometry*, pp. 237–249, 2006.
[32] K. Nordmeyer, “Bestimmung von Strontium-90 in Lebensmitteln nach Extraktionschromatographie mit Eichrom-Harz,” *Lebensmittel- und Veterinärinstitut*

Oldenburg, Niedersächsisches Landesamt für Verbraucherschutz und Lebensmittelsicherheit, 2016.

[33] L. Brüggemann, W. Quapp, and R. Wennrich, “Test for non-linearity concerning linear calibrated chemical measurements,” *Accred Qual Assur*, vol. 11, no. 12, pp. 625–631, 2006.

[34] *Chemical analysis - Decision limit, detection limit and determination limit under repeatability conditions - Terms, methods, evaluation*, DIN 32645:2008-11, 2008.

[35] *German standard methods for examination of water, waste water and sludge - General information (group A)-Part 51: Calibration of analytical methods - Linear calibration (A 51)*, DIN 38402-51:2014-05, 2014.

[36] *Determination of the characteristic limits (decision threshold, detection limit and limits of the confidence interval) for measurements of ionizing radiation- Fundamentals and application*, DIN ISO 11929:2011-01, 2011.

[37] Bundesamt für Strahlenschutz, “Dosiskoeffizienten bei innerer Strahlenexposition für Einzelpersonen der Bevölkerung,” pp. 1689–1876.

[38] E. C. Anderson, R. L. Schuch, W. Langham, and W. R. Fisher, “Radioactivity of People and Foods,” *Science*, vol. 125, no. 3261, pp. 1273–1278, 1957.

[39] T. Rahola and Suomela M., “On biological half-life of potassium in man.,” *Annals of Clinical Research*, vol. 2, no. 7, 1975.

6. Appendix

Appendix A: List of abbreviations

Abbreviation	Meaning
$\hat{y}_i$	y values of regressive linear calibration
$\dot{U}$	Annual food consumption
$s_{e,1}^2$	Variance of linear function
$s_{e,2}^2$	Variance of quadratic function
$\overline{x}$	mean of *x* values
a	gradient
A	specific activity
A(t)	Activity
$A_{m,R}$	Activity concentration
b	slope
bis-MSB	1,4-bis(2-methylstryryl)benzole
Bq	Becquerel
BWR	Boiling water reactor
C	Channel
CCS	Containment Cooling
CI	confidence interval
CS	Core Spray system
DIN	diisopropylnaphthaline
$D_{T,R}$	Adsorbed dose
E	Effective dose
E(C)	Energy of channel
ECCS	Emergency core cooling system
E_{ing}	Effective ingestion dose
eV	Electron volt

Abbreviation	Meaning
FWHM	Full-width half maximum
$F_{\alpha,1,N-3}$	F-test parameter
$g_{ing,r}$	Dose coefficient
GUM	Guide to the Expression of Uncertainty in Measurement
Gy	Gray
HPCI	High-pressure Coolant injection System
HPGe	High-purity germanium
HPGe	High-purity germanium
$H_{T,R}$	Equivalent dose
IC	Isolation condensor
ICP MS	Inductively coupled plasma mass spectrometry
ICP-OES	Inductively coupled plasma atomic emission spectroscopy
INES	International Nuclear and Radiological Event Scale
k	Equilibrium constant
k_s	summation correction factor
LOD	limit of detection
LOQ	limit of quantification
LSC	Liquid scintillation counter
M	number of repeat measurements
m	sample mass
MOX	Mixed oxides
MW	Mega watt
N	Number of calibration standards
N(t)	quantity of nucleus at time *t*

Abbreviation	Meaning
LSC	Liquid scintillation counter
M	number of repeat measurements
m	sample mass
MOX	Mixed oxides
MW	Mega watt
N	Number of calibration standards
N(t)	quantity of nucleus at time *t*
N_0	initial quantity of the nuclei
NPP	Nuclear Power Plant
Ø	diameter
PCR	Primary containment vessel
PMT	Photomultiplier
PPO	2,5-Diphenoloxazol
p_γ	gamma emission probability
R	Type of radiation (α,β,γ,n,..)
r_0	zero effect count rate
RCIC	Reactor core isolation cooling system
r_{emit}	gamma emission rate
RHR	Residual heat removal system
r_{ini}	initial area count rate
r_n	net count rate
RPV	Reactor pressure vessel
s_a	standard deviation of gradient
s_e	residual standard deviation
SEM	Secondary electron multiplier
Sv	Sievert
T	tissue
t	time
$t_{1/2}$	half-life
TDCR	Triple-to-double coincidence ratio
TEPCO	Tokyo Electric Power Company
t_{exp}	Time of exposition

Abbreviation	Meaning
$u(x_i)$	uncertainty of
w_r	Radiation weighting factor
w_T	Specific weighting factor for tissue
X_D	Daughter nuclide
X_P	Parent nuclide
Y	stable decay product
y_{crit}	critical y-value
y_i	y values of measurement
β_{End}	Beta end point energy
λ	Decay rate
σ	Neutron capture cross section
τ	mean lifetime
ω	Mass fraction
ϵ	efficiency

Appendix B: List of figures

Figure 1: a) Location of the Fukushima Daiichi NPP in Japan. The grey area is the prefecture Fukushima with its capital Fukushima. The epicentre of the earthquake on the 11th March 2011 was east of the city of Sendai. b) Fukushima Daiichi NPP area with the location of the six reactor units. 1 b) modified after [7]. 2
Figure 2: Profile of Daiichi NPP Unit 1 with the reactor building directed towards the land mass and with the affiliated power house towards the sea. The height of the tsunami wave and the height of the protection wall are indicated. Modified after [7]. 3
Figure 3: The rating system of the international nuclear and radiological event scale (INES). 8
Figure 4: Deposits of cumulated cesium activity released during Fukushima Daiichi NPP nuclear accident. Estimated effective doses from external radiation from specific regions are labelled with red lines [13] 10
Figure 5: secular equilibrium of ^{90}Sr with ingrowing daughter nuclide ^{90}Y. 12
Figure 6: ^{90}Sr decay scheme. ^{90}Sr is a pure emitter with a half time of 28.79 a and decays to ^{90}Y. Due to the short half time of ^{90}Y (64 h), the parent and daughter radionuclide form a sequiliar equilibrium. ^{90}Y decay into the stable ^{90}Zr 17
Figure 7: Annual food consumption of Japanese people. 20
Figure 8: Molecular structure of strontium binding 4,4'(5')-di-*t*-butylcyclohexano-18-crown-6. The Sr binds at high pH values with two coordinated nitrate anions and is released at lesser pH values. 22
Figure 9: LSC beta spectra of ^{85}Sr, ^{90}Sr and ^{90}Y with characteristic spectra lines for each radionuclide and blank. The three windows for analysis are separated with red lines. The direct analysis for ^{90}Sr is done with window 2, whereas after 14 days the activity determination of the combined activity of ^{90}Sr and ingrown ^{90}Y is done with window 2 and 3. Window 1 can be used for yield determination with ^{85}Sr. 25
Figure 10: Liquid scintalliation counter (LSC) Hidex 300 SL from Hidex OY with TDCR technology. 28
Figure 11: Sampling location of different kinds of food across Japan. Manufactured foods, where the original location is unknown, are not represented in the map. 29
Figure 12: Chemical yield of ^{85}Sr in dependence of the time of elution from Sr resin. 33
Figure 13: LSC measurement calibration curves for a) Window 2 (Channel 281 – 680) for the determination of ^{90}Sr in freshly separated samples and b) Window 2 + 3 (Channel 281 - 820) for the activity determination of ^{90}Sr and ingrown daughter nuclide ^{90}Y. 35
Figure 14: Location of specific analysed food samples in January 2016 with significant radiocesium contamination, mainly mushrooms. In a 300 km radius around the location of the Fukushima NPP accident, the short lifed ^{134}Cs ($t_{1/2}$ = 2.065 a) can be determined. The ratio ^{134}Cs/^{137}Cs calculated back to the time of the Fukushima NPP accident is 1 and therefore

characteristic for the accident. Samples from further away have values of ^{134}Cs below the detection limit; this allows the attribution of the ^{137}Cs to atmospheric nuclear weapon fallout.44

Appendix C: List of tables

Table 1: Properties of the reactor units of the Fukushima Daiichi NPP [7]..... 2
Table 2: Amount of fuel inside the units at the time of accident on the 11th of March 2011 [7, 9]. 4
Table 3: Medium and long lived fission product yields for most commonly used ^{235}U and ^{239}Pu with fission inducing thermal neutron [18]. 16
Table 4: Japanese established limits of radionuclides in food [26]. 21
Table 5: Temperature programme of the 1st and 2nd incineration step..... 31
Table 6: Chemical yield of the preparation steps. 32
Table 7: Parameters of the calculation of the limit of detection and quantification for the calibration function for ^{90}Sr and for ^{90}Sr/^{90}Y..... 36
Table 8: ^{90}Sr spiked test solutions with the calculated and chemical yield corrected activity. ... 37
Table 9: The analyzed 37 food concentrated from Japan ordered after the food category and their distances to the Fukushima Daiichi NPP. Furthermore, the mass of the raw portion and the determined ^{90}Sr/^{90}Y activity is given. *marked foods have added radiotracer ^{85}Sr and the Compton background was corrected for the analysis. 39
Table 10: The calibration standard QCY-48 from Eckert & Ziegler Isotope Products is from 1st May 2016. The standard solution was soluted with a factor of 0.0255. * ^{203}Hg was almost completely decayed at time of usage of the standard. For this reason, it was not considered for energy, efficiency or activity calculations. 40
Table 11: Determined specific activities of ^{134}Cs, ^{137}Cs and ^{40}K in various foods, ordered after food category and in dependence on distance to the Fukushima NPP. In red: radiocesium contamination above the legal limit of 100 Bq/kg. 43
Table 12: Radiosilver specific activity in seafood samples, measurement results from Katsumi Shozugawa (Appendix …). 46
Table 13: Estimation of the worst-case annual ingestion dose, resulting from consumption of the analysed 37 samples. The calculation used the highest found radionuclide contamination in the samples and it was extrapolated to the food consumption of Japanese people from [25]. *including mushrooms. **in respect to the detection limit with the smallest analysed mass of sample in the food category. 47
Table 14: The effective half-life of radionuclides ^{90}Sr, ^{134}Cs, ^{137}Cs and ^{40}K inside the organism and the calculated effective dose in the following 10 years after one-time annual ingestion.... 48

Appendix D: Additional information

Exact information of each sample with data by Dr. Katsumi Shozugawa, University of Tokyo.

no on tubes	Sample	distance from Fukushima plant [km]	Collected/ Produced Points	Concentration by heating	live time [sec]	Day back (just equivalent to day of sampling)	^{134}Cs [Bq/kg$_{raw}$9	^{134}Cs_error	^{137}Cs[Bq/kg$_{raw}$]	^{137}Cs_error	^{40}K [Bq/kg]	^{40}K_error	$^{134/137}$Cs ratio as of the accident	error
1	Coffee	-	Instant coffee produced before March 2011	-	228000	2015-05-29	ND(0.22)		6.24E-01	5.90E-02	1.21E+03	5.30E+00	-	-
2	Dorado	217	from Chiba (except bones/the internal organs)	14.09 kg → 2.777 kg	53902	2015-06-01	3.26E-02	9.15E-03	2.66E-01	1.23E-02	1.15E+02	7.75E-01	0.460	0.131
3	Bonito	-	from Miyagi. the Pacific Ocean	9.680 kg → 2.696 kg	236300	2015-04-28	1.02E-01	4.50E-03	5.07E-01	9.66E-03	1.15E+02	4.91E-01	0.733	0.035
4	sweet potato	127	from Ibaraki	12.550 kg → 4.430 kg	80000	2015-04-09	3.33E-01	1.04E-02	1.20E+00	2.46E-02	1.34E+02	9.18E-01	0.996	0.037
5	Japanese tee	401	from Kakegawa. Shizuoka	-	70000	2015-06-02	3.61E-01	3.18E-02	1.32E+00	6.04E-02	4.36E+02	3.42E+00	1.027	0.102
6	mushroom	491.1	from Hokkaido. Hen of the Woods	-	150000	2015-06-27	ND(1.35)		3.77E+00	3.84E-01	5.64E+02	1.49E+01	-	-
7	carrot	217	From Chiba	22.85 kg → 1.924 kg	80000	2015-07-21	2.76E-02	3.38E-03	1.16E-01	5.18E-03	9.36E+01	4.08E+00	0.932	0.122
8	peanuts	217	From Chiba	2.012 kg → 1.925 kg	50000	2015-07-27	2.57E-01	2.72E-02	1.15E+00	6.27E-02	2.13E+02	2.76E+00	0.883	0.105
9	flatfish	95.2	from Miyagi. the Pacific Ocean	13.30 kg → 2.793 kg	154450	2015-08-01	ND(0.02)		5.17E-02	5.91E-03	9.40E+01	4.93E-01	-	-
10	skimmed milk	-	by Morinaga company	-	63500	2015-09-15	3.33E-01	3.44E-02	1.43E+00	7.07E-02	5.13E+02	4.27E+00	0.958	0.110
11	blueberry	181	from Ibaraki	9.499 kg → 1.359 kg	80600	2015-09-04	2.92E-02	3.59E-03	1.07E-01	5.93E-03	2.30E+01	2.77E-01	1.114	0.151
12	sea water	0.6	600 m south of Fukushima NPP	12.640 kg → 2.253 kg	160289	2014-03-19	2.39E-01	4.79E-03	6.26E-01	7.74E-03	1.09E+01	1.23E-01	0.982	0.023
13	rice	15.9	from Naraha. Fukushima	-	310800	2015-11-20	1.71E-01	7.51E-03	7.44E-01	1.66E-02	2.24E+01	3.76E-01	0.997	0.049
14	rice	11.1	from Namiem. Fukushima	-	80000	2015-12-04	1.46E-01	1.54E-02	7.08E-01	3.32E-02	1.92E+01	6.57E-01	0.910	0.105
15	mushroom	306	From Kanagawa. Shiitake mushroom	-	67550	2016-01-04	2.63E+01	1.85E-01	1.20E+02	5.77E-01	5.78E+02	4.96E+00	0.986	0.008
16	mushroom	95.2	from Miyagi. Cortinarius praestans	2570 g → 90.0 g	6120	2016-01-26	3.21E+00	1.59E-01	1.47E+01	4.79E+01	5.47E+00	1.56E+00	1.003	0.060

no on tubes	Sample	distance from Fukushima plant [km]	Collected/ Produced Points	Concentration by heating	live time [sec]	Day back (just equivalent to day of sampling)	^{134}Cs [Bq/kg$_{raw}$]	^{134}Cs_error	^{137}Cs [Bq/kg$_{raw}$]	^{137}Cs_error	^{40}K [Bq/kg]	^{40}K_error	$^{134/137}$Cs ratio as of the accident	error
17	sardines	127	from Ibaraki. the Pacific Ocean	8.240 kg → 2.439 kg	33720	2016-02-12	1.55E-01	1.74E-02	8.03E-01	3.37E-02	3.66E+02	2.15E+00	0.903	0.108
18	squid	346.9	from Aomori	15.065 kg → 2.773 kg	653640	2016-02-17	7.43E-03	1.42E-03	6.14E-02	2.26E-03	7.85E+01	1.91E-01	0.567	0.111
19	pond smelt	160.4	From Ibaraki	312 g → 147 g	14400	2016-02-26	2.82E+00	2.67E-01	1.24E+01	7.12E-01	5.73E+01	6.82E+00	1.079	0.119
20	brown rice	217	From Chiba	10.020 kg → 2.540 kg	219101	2016-02-26	4.36E-02	3.95E-03	2.01E-01	7.12E-03	8.14E+01	4.32E-01	1.027	0.100
21	taro	111.7	from Yamagata	14.40 kg → 1.922 kg	68860	2016-03-14	4.81E-02	4.22E-03	2.42E-01	8.64E-03	1.36E+02	5.96E-01	0.952	0.090
22	rice	230.8	from Gumma	8.145 kg → 1.990 kg	431350	2016-03-17	1.44E-02	2.12E-03	7.46E-02	3.49E-03	2.91E+01	2.00E-01	0.930	0.143
23	mushroom	189	from Gumma	300 g → 29.0 g	11499	2016-02-23	3.71E+00	2.02E-01	1.77E+01	5.69E-01	7.88E+01	4.95E+00	0.991	0.063
24	tuna	374.4	from Shizuoka. the Pacific Ocean	-	513435	24.03.2016	6.65E-02	1.66E-02	5.67E-01	1.80E-02	2.77E+02	1.14E+00	0.568	0.143

New samples from Dr. Katsumi Shozugawa

no on tubes	Sample	distance from Fukushima plant [km]	Collected/ Produced Points	Concentration by heating r=raw/dried	live time [sec]	Day back (just equivalent to day of sampling)	^{134}Cs [Bq/kg$_{raw}$]	^{134}Cs_error	^{137}Cs [Bq/kg$_{raw}$]	^{137}Cs_error	^{40}K [Bq/kg]	^{40}K_error	$^{134/137}$Cs ratio as of the accident	error	^{108m}Ag [Bq/kg$_{raw}$]	^{108m}Ag_error	^{110m}Ag [Bq/kg$_{raw}$]	^{110m}Ag_error
1	oyster	95	from Miyagi. 2015	r=9.707	507650	2016-06-07	1.03E-02	1.27E-03	6.01E-02	2.24E-03	3.58E+01	1.54E-01	8.88E-01	1.14E-01	8.92E-03	1.61E-03	5.68E-02	1.49E-03
2	baked sea-weed	695	from Setouchi (Seto Island). 2016	-	84000	2016-06-30	ND(0.26)		ND(0.27)		9.61E+02	6.10E+00						
3	white-bait (Shirasu)	1071	from Miyazaki. 2016	r=4.115	167840	2016-07-05	ND(0.018)		5.30E-02	5.13E-03	8.77E+01	4.32E-01						
4	boiled fish paste	-	by Kibun company	r=2.66	1141430	2016-07-07	ND(0.01016)		7.26E-03	2.48E-03	3.63E+01	1.74E-01						
5	wheat	254	from Iwate. 2016	-	300000	2016-08-04	MD(0.026)		1.06E-01	1.12E-02	3.36E+01	4.92E-01						
6	rice (Brown rice)	40.4	from Tamura. Fukushima. 2016	-	24410	2016-08-19	2.57E-01	3.28E-02	1.30E+00	8.10E-02	6.69E+01	2.10E+00	1.09E+00	1.54E-01				
7	rice (Brown rice)	201	from Shiroi. Chiba. 2015	-	79640	2016-08-31	2.49E-01	1.74E-02	1.40E+00	4.49E-03	6.72E+01	1.14E+00	9.86E-01	6.90E-02				
8	wild boar jerkey	335	from Izu. Shizuoka. 2016	r=1.3464	14400	2016-09-02	5.94E+00	6.23E-01	3.17E+01	1.78E+00	2.84E+02	2.22E+00	1.04E+00	1.24E-01				
9	blueberry paste	214	from Saitama	r=7.2782	20620	2016-09-14	1.36E-01	8.72E-03	7.69E-01	2.66E-02	2.45E+01	5.62E-01	9.96E-01	7.20E-02				
10	Inonotus obliquus	3600	Russian mushroom	-	28911	2016-09-20	ND(0.62)		4.34E+01	6.36E-01	1.68E+03	1.51E+01						
11	Ablone (Awabi)	629	from Hokkaido. 2016	r=4.4043	76640	2016-09-26	ND(0.027)		3.35E-02	7.38E-03	8.22E+01	5.93E-01			3.22E-02	5.13E-03		
12	Ablone (Awabi) Log grown	218	from Chiba. 2016. from Iwaki. Fukushima. 2016	r=4.031	96570	2016-09-30	ND(0.024)		ND(0.028)		6.25E+01	5.25E-01			3.27E-02	7.69E-03		
13	mushroom	35	Shiitake mushroom	r=11.067	91430	2016-09-24	3.69E-01	4.07E-02	2.45E+00	9.32E-02	6.27E+01	1.89E+00	8.54E-01	1.00E-01				

^{85}Sr calibrations curve:

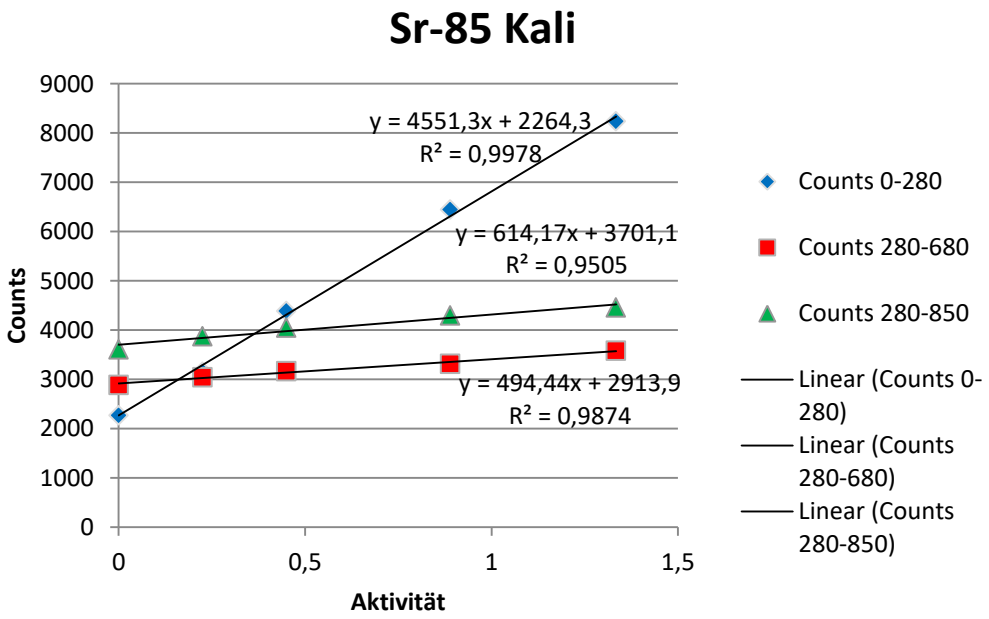

Appendix E: Certificates

Characteristics of used HPGe Detector 1. 3. 5

Detector 1

Instrument type	**GMX Series HPGe GAMMA-X HPGe**	
Germanium crystal type	Diameter:	59.9 mm
	Length:	53.5 mm
	Depletion layer:	5 mm
Window	Material:	Beryllium
	Thickness:	0.5 mm

Detector 3

Instrument type	**GEM Series HPGe Coaxial Detector System**	
Germanium crystal type	Diameter:	62 mm
	Length:	75 mm
	Depletion layer:	3 mm
Window	Material:	Aluminum

	Thickness:	1.0 mm

Detector 5

Instrument type	**CANBERRA Low Energy Germanium Detector**	
Germanium crystal type	Diameter:	60 mm
	Length:	20 mm
	Depletion layer:	5 mm
Window	Material:	Carbon Epoxy
	Thickness:	0.5 mm

QCY-48 standard certificate segment

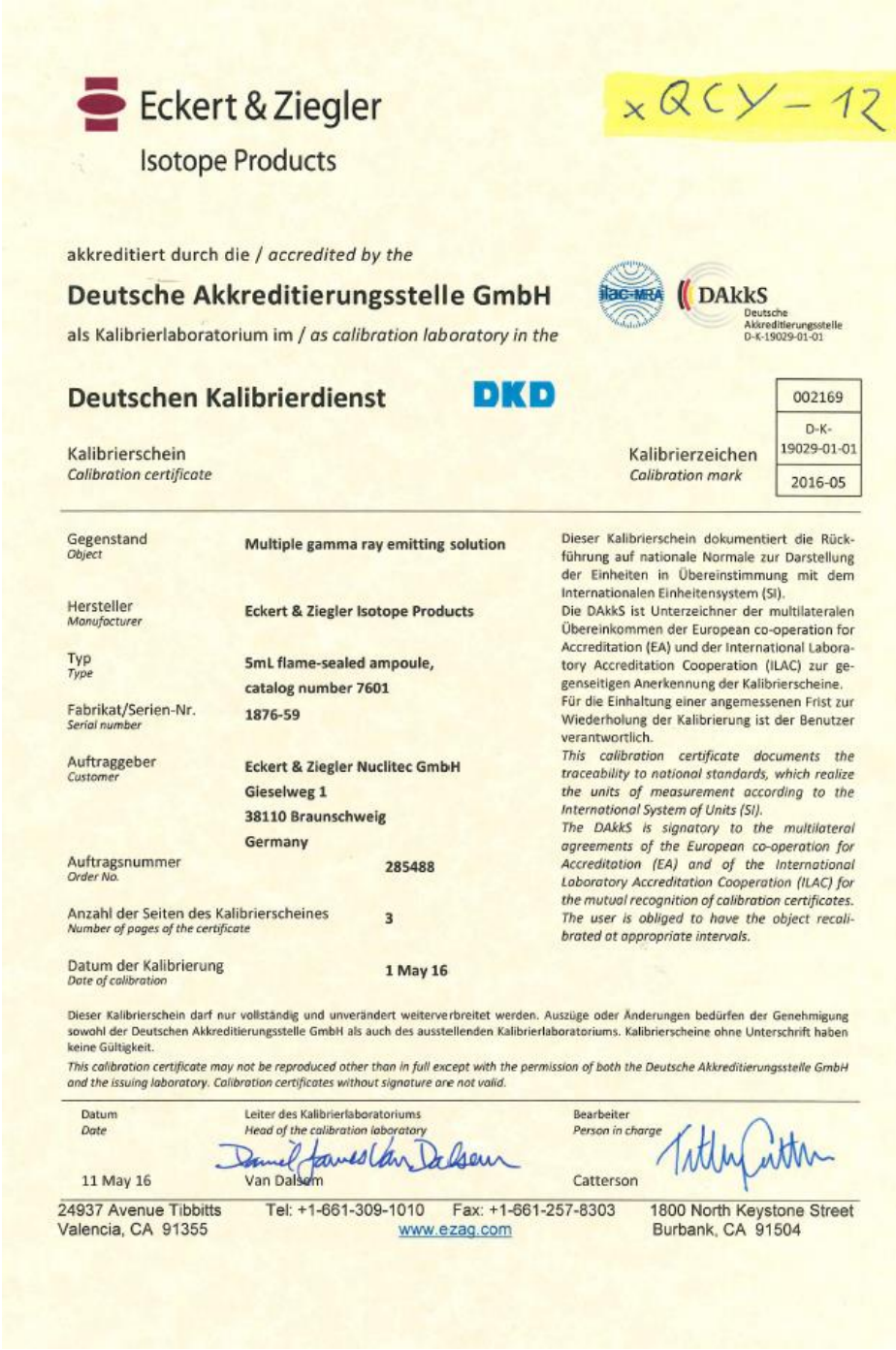

Eckert & Ziegler
Isotope Products

xQCY-12

akkreditiert durch die / *accredited by the*

Deutsche Akkreditierungsstelle GmbH

als Kalibrierlaboratorium im / *as calibration laboratory in the*

DAkkS Deutsche Akkreditierungsstelle D-K-19029-01-01

Deutschen Kalibrierdienst DKD

Kalibrierschein *Calibration certificate*	Kalibrierzeichen *Calibration mark*
	002169
	D-K-19029-01-01
	2016-05

Gegenstand *Object*	**Multiple gamma ray emitting solution**
Hersteller *Manufacturer*	**Eckert & Ziegler Isotope Products**
Typ *Type*	**5mL flame-sealed ampoule, catalog number 7601**
Fabrikat/Serien-Nr. *Serial number*	**1876-59**
Auftraggeber *Customer*	**Eckert & Ziegler Nuclitec GmbH** **Gieselweg 1** **38110 Braunschweig** **Germany**
Auftragsnummer *Order No.*	**285488**
Anzahl der Seiten des Kalibrierscheines *Number of pages of the certificate*	**3**
Datum der Kalibrierung *Date of calibration*	**1 May 16**

Dieser Kalibrierschein dokumentiert die Rückführung auf nationale Normale zur Darstellung der Einheiten in Übereinstimmung mit dem Internationalen Einheitensystem (SI).
Die DAkkS ist Unterzeichner der multilateralen Übereinkommen der European co-operation for Accreditation (EA) und der International Laboratory Accreditation Cooperation (ILAC) zur gegenseitigen Anerkennung der Kalibrierscheine.
Für die Einhaltung einer angemessenen Frist zur Wiederholung der Kalibrierung ist der Benutzer verantwortlich.

This calibration certificate documents the traceability to national standards, which realize the units of measurement according to the International System of Units (SI).
The DAkkS is signatory to the multilateral agreements of the European co-operation for Accreditation (EA) and of the International Laboratory Accreditation Cooperation (ILAC) for the mutual recognition of calibration certificates. The user is obliged to have the object recalibrated at appropriate intervals.

Dieser Kalibrierschein darf nur vollständig und unverändert weiterverbreitet werden. Auszüge oder Änderungen bedürfen der Genehmigung sowohl der Deutschen Akkreditierungsstelle GmbH als auch des ausstellenden Kalibrierlaboratoriums. Kalibrierscheine ohne Unterschrift haben keine Gültigkeit.

This calibration certificate may not be reproduced other than in full except with the permission of both the Deutsche Akkreditierungsstelle GmbH and the issuing laboratory. Calibration certificates without signature are not valid.

Datum *Date*	Leiter des Kalibrierlaboratoriums *Head of the calibration laboratory*	Bearbeiter *Person in charge*
11 May 16	Van Dalsem	Catterson

24937 Avenue Tibbitts
Valencia, CA 91355
Tel: +1-661-309-1010 Fax: +1-661-257-8303
www.ezag.com
1800 North Keystone Street
Burbank, CA 91504

6.4.2.4 Sr-Resin certificate

ANALYSEN-ZERTIFIKAT

N° CA-R- FSRS160719

Produkt: Resin SR Grade S Granulometrie: 50-100 µm
Lot # FSRS160719

Dieses SR Resin Lot wurde gemäß den TrisKem Standard-Arbeitsanweisungen hergestellt. Das Lot wurde gemäß TrisKems Qualitätskontrollprozeduren und -regeln getestet. Dieses Lot entspricht in allen Punkten TrisKems Qualitätsanforderungen. Dieses Resin unterliegt einer Garantie von zwei Jahren gültig ab dem Lieferdatum.

ANALYSEN ERGEBNISSE

Tests	Anforderung	Ergebnis
Aussehen	weisse Kugeln	konform
Gesamtkohlenstoff im Eluat (NPOC Methode) in µg.mL^{-1}	≤ 25	23,9
Maximale Sr Kapazität in 3.1 M HNO_3 in mg Sr.g^{-1} Resin	≥ 25	26,8
% Sr eluiert in 0.05M HNO_3 (5 Replikate)		
Kleinster akzeptabler Mittelwert in %	≥ 85,0	91,5
Max. Standardabweichung in %	≤ 2,5	0,7
% Ca eluiert in 0.05M HNO_3 (5 Replikate)		
Grösster akzeptabler Mittelwert in %	≤ 0,5	0,1
Max. Standardabweichung in %	≤ 0,25	0,1
% Ba eluiert in 0.05M HNO_3 (5 Replikate)		
Grösster akzeptabler Mittelwert in %	≤ 0,5	0,3
Max. Standardabweichung in %	≤ 0,25	0,2
% Y eluiert in 0.05M HNO_3 (5 Replikate)		
Grösster akzeptabler Mittelwert in %	≤ 0,5	0,0
Max. Standardabweichung in %	≤ 0,25	0,0
% Y eluiert in 8M HNO_3 (5 Replikate)		
Kleinster akzeptabler Mittelwert in %	≥ 95,0	95,7
Max. Standardabweichung in %	≤ 2,5	2,0

Herstellungsdatum Resin: 19/07/2016
Herstellungsdatum Kartuschen: 29/09/2016

25/10/2016
Datum

Steffen Happel
Qualitätskontrolbeauftragter

Version en vigueur	Stockage	Accès	Conservation	page
11/02/2016	Informatique - papier	Libre	5 ans	1/1

TRISKEM INTERNATIONAL
ZAC de l'Eperon – 3, rue des Champs Géons – 35170 Bruz – FRANCE
Tel +33 (0)2.99.05.00.09 – Fax +33 (0)2.23.45.93.19 – www.triskem.com – email : contact@triskem.fr
SAS au capital de 40.000 euros – SIRET 493 848 972 00029 – APE 2059Z – TVA intra communautaire FR65 493 848 972

Appendix F: Selbstständigkeitserklärung

Hiermit erkläre ich. dass die von mir vorgelegte Masterarbeit zum Thema “Determination of Sr-90 in food concentrates from Japan” selbstständig verfasst wurde und die verwendeten Quellen und Hilfsmittel im Text gekennzeichnet wurden.

Hannover. der März 2017

_____

(Anica Weller)